

LANDAU-FLUID CLOSURES AND NUMERICAL
IMPLEMENTATION IN BOUT++

A Thesis Submitted to the
College of Graduate and Postdoctoral Studies
in Partial Fulfillment of the Requirements
for the degree of Master of Science
in the Department of Physics & Engineering Physics
University of Saskatchewan
Saskatoon

By

Oleksandr Chapurin

©Oleksandr Chapurin, September 2017. All rights reserved.

PERMISSION TO USE

In presenting this thesis in partial fulfilment of the requirements for a Postgraduate degree from the University of Saskatchewan, I agree that the Libraries of this University may make it freely available for inspection. I further agree that permission for copying of this thesis in any manner, in whole or in part, for scholarly purposes may be granted by the professor or professors who supervised my thesis work or, in their absence, by the Head of the Department or the Dean of the College in which my thesis work was done. It is understood that any copying or publication or use of this thesis or parts thereof for financial gain shall not be allowed without my written permission. It is also understood that due recognition shall be given to me and to the University of Saskatchewan in any scholarly use which may be made of any material in my thesis.

Requests for permission to copy or to make other use of material in this thesis in whole or part should be addressed to:

Head of the Department of Physics & Engineering Physics

Rm 163

116 Science Place

University of Saskatchewan

Saskatoon, Saskatchewan

Canada

S7N 5E2

ABSTRACT

Fluid models are used to quantitatively describe many phenomena in plasmas, providing a reduced description of the lower dimensionality in comparison to kinetic models. Often, fluid models are more amenable to numerical and analytical analysis including nonlinear effects. The principal drawback of fluid models is the inability to describe kinetic effects which are important in the long mean free path regimes. However, a linear closure can be introduced to model kinetic effects, such as Landau damping. Such closures for three- and four-moment fluid model [G.W. Hammett and F.W. Perkins, *Physical Review Letters* **64**, 3019(1990)] are known to be able to model plasma response function (with the decent accuracy) and kinetic effects of plasma microinstabilities (such as ion-temperature gradient instability). One of the results of this work is the derivation of the exact linear closure for the set of one-dimensional plasma fluid equations. The exact linear expression for the heat flux is obtained thus replacing the infinite hierarchy of fluid moments with a finite set of equations that incorporate kinetic effects of thermal motion into a fluid model. It is shown that the obtained exact closure in the limit case is reduced to the closure derived previously by Hammett and Perkins. Another goal of this work is to show how such fluid model with the kinetic closure can be modeled numerically using a recently developed non-Fourier method [A. Dimits, et. al., *Phys Plasmas*, **21** (5) 2014]. The method is based on the approximation of a Fourier image by a sum of Lorentzian functions allowing fast conversion into the configuration (real) space. With this approach, the one-dimensional model which includes evolution equation for the energy was implemented using the BOUT++ framework. The numerical implementation was verified in the series of test simulations of the plasma response function. Additionally, a self-consistent model of the ion Landau damping was implemented. It is shown that the damping rate for the ion Landau damping model agrees well with the exact kinetic result.

ACKNOWLEDGEMENTS

I would like to express my gratitude to my supervisor Professor Dr. Andrei Smolyakov. Thank you for introducing me to the plasma physics research, for guiding me in developing my Master's thesis, and for the useful comments, remarks, and engagement through my studies. I also want to thank Dr. Maxim Umansky, for his visit to U of S and constant help with BOUT++, which allows mastering my skills. Thanks to the members of my committee for their great suggestions that have notably improved this thesis. Also, my fellow graduate students at the U of S, I have learned from you so much a lot, you created an exceptional research atmosphere.

My special thanks are to my family, in particular to my mother and brother. From our long and winding road together I have learned never to give up and bridge over all the difficulties.

CONTENTS

Permission to Use	i
Abstract	ii
Acknowledgements	iii
Contents	iv
List of Figures	vi
1 Introduction	1
1.1 Plasma models	4
1.1.1 Kinetic plasma equations: Boltzmann and Vlasov models	4
1.1.2 Particle-in-cell method	8
1.1.3 Fluid plasma equations	9
1.1.4 Collisional closures for fluid equations	14
1.2 Waves in plasmas	17
1.2.1 Ion sound waves	17
1.2.2 Electrostatic waves in kinetic theory and ion Landau damping	19
2 One-dimensional collisionless closures	30
2.1 Hammett-Perkins closure	30
2.1.1 Three-moment Landau-fluid closure	31
2.1.2 Four-moment Landau-fluid closure	32
2.2 Closure model for the heat flux	33
2.2.1 One-dimensional moment equations	33
2.2.2 Chapman-Enskog method for heat flux closure derivation	35
2.3 Ion sound dispersion relation from the fluid model with the closure	39
3 Numerical implementation of collisionless closures	41
3.1 Fast non-Fourier method for the computation of closure operators	42
3.2 BOUT++: High Performance fluid simulations framework	43
3.3 Evaluation of plasma response function	47
3.3.1 Three-moment Landau-fluid model	48
3.3.2 Improvement to the three-moment kinetic closure	51
3.3.3 Four-moment Landau-fluid model	52
3.4 Landau damping with kinetic closure	53
4 Conclusion	56
References	59

A	Generalized closure for the viscosity and heat flux in 3D case	63
B	Plasma dispersion function	70
C	Velocity weighted integrals of the Maxwellian in terms of Plasma Dispersion Function	73

LIST OF FIGURES

1.1	Types of distribution function in 2D (v_x, v_y) phase space, represented with the contour lines of a constant velocity distribution function (arbitrary units). The examples (a), (b), and (c) do not involve the higher-order moments, like the heat flux; (d) is the example of the distribution function with a finite heat flux.	6
1.2	Phase space evolution for two-stream instability, initialized with the two counter-streaming Maxwellian beams. Beams are represented with black (moving in the negative direction) and blue (moving in the positive direction) dots. System also includes immobile ion's background. Velocity v and coordinate x units are shown in normalized units. Later in the simulation, (d), (e) and (f), the system enters the strongly nonlinear stage with particle trapping and multivalued solutions. These regimes cannot be described by the linear closures studied in this thesis.	10
1.3	Complex plane with contour lines of $\text{Im}(R) = 0$ (red) and $\text{Re}(R) = -\tau$ (black) for values of $\tau = 0.1, 0.4, 0.7, 1.0, 1.3, 1.6$. Roots with the smallest $ \text{Im } \omega $ are circled.	23
1.4	Landau damping for ion sound waves. Exact solution of Eq. (1.89) represented with solid line, approximate solution (1.101) with a dashed line.	25
1.5	Landau damping of an electrostatic wave for two different initial distributions: (a) "quiet start" with a well represented Maxwellian; (b) random Maxwellian distribution.	26
1.6	Velocity distribution function produced with two methods of initial particle loading in the XES1 code: quiet start technique (solid) and random particle distribution (dashed).	27
1.7	Conservation of energy in the simulation of Landau damping. Energy from the initial electrostatic wave (dashed line) has been transferred to particles kinetic energy (solid line). Energy units are normalized.	28
1.8	Phase-space evolution of the electron component of the plasma during the Landau damping simulation. Due to symmetry, only the positive velocity region plotted. Linear regime is characterized by shearing of the initial perturbation (b), in nonlinear regime particle trapping occurs (holes in phase space) which stops damping, (c)-(d). The linear closures are not valid in strongly nonlinear regimes.	29
2.1	The real and imaginary parts of the normalized response function $R(\zeta)$ versus the normalized real frequency ζ	34
2.2	Exact kinetic response function presented here with solid lines, HP four-moment LF with dashed lines and our Chapman-Enskog closure (dotted lines) in the first-order approximation, Eq. (2.42).	38

2.3	Landau damping for three-moment fluid model with kinetic closure (2.46). The exact solution of the dispersion equation (2.49) (red) and the approximate solution (2.52) (red dashed) in comparison with the exact kinetic solution of Eq. (1.89) (blue dashed).	40
3.1	Plot of $ k \psi_7(k)$, where $\psi_7(k)$ (3.3) is the approximation for $1/ k $. Therefore, region of good fit is around one; (a) shows a wide range of wavenumber values, including regions, where approximation becomes not valid; (b) represents the same plot within range of good fit.	43
3.2	Plot of $ k \psi_7(k)$, where $\psi_7(k)$ (3.3) is the approximation for $1/ k $. It can be “shifted” into lower and higher wavenumber region using a multiplier k_0 for α in Eq. (3.3); solid blue line corresponds to $k_0 = 1$	44
3.3	Overview of the BOUT++ code control flow during initialization (red) and during running (blue).	45
3.4	Plasma density response for externally driven potential, for several driven frequencies. The different amplitude response (smaller for higher frequency) can be noted. The solution settles to the constant sine form after ~ 10 ion plasma periods, after what the evaluation of the plasma response function (3.8) can be performed.	50
3.5	The plasma density response \tilde{n} for the externally driven potential $\tilde{\phi}_{ext} \sim \sin(2\omega_{pi}t)$. The phase shift δ between the driven wave and the response, along with the amplitude A of the density response are used to evaluate the plasma response function (3.8).	51
3.6	The real and imaginary parts of the normalized response function for the three-moment model (with BOUT++ non-Fourier calculations) with HP-like closure (3.11) compared to the exact response function.	52
3.7	The real and imaginary parts of the normalized response function for the three-moment model (with BOUT++ non-Fourier calculations) with improved closure (3.17) compared to the exact response function.	53
3.8	The real and imaginary parts of the normalized response function for the four-moment model (with BOUT++ non-Fourier calculations) with HP-like closure (3.19) compared to the exact response function.	54
3.9	Landau damping for three-moment fluid simulation with kinetic closure. Numerical result (circles) for damping rate in comparison with exact solution of the fluid dispersion relation (2.49) (solid red). Also, the exact kinetic solution of ion Landau damping is presented (dashed blue).	55
A.1	The real and imaginary parts of the normalized plasma response function. Three-moment model with Litt-Smolyakov closure (A.29) response function R3LS (dotted) is compared to the Hammett-Perkins three-moment response function result R3HP (dashed). The exact plasma response function R is also present (solid).	69
B.1	Plasma dispersion function for the real argument.	71
B.2	Plasma dispersion function for the complex argument with positive imaginary values; (a) shows the real output and (b) shows the imaginary output.	71

B.3 Plasma dispersion function for the complex argument with negative imaginary values.	72
---	----

CHAPTER 1

INTRODUCTION

Plasma is a quasineutral gas of charged particles in which particle interactions are predominantly collective due to long-range electromagnetic forces. Collective effects are responsible for a plethora of physical phenomena such as waves, instabilities, turbulence, and transport. Dynamics of plasma involve electromagnetic forces and classical equations of motion. Quantum effects in plasma are important when the de Broglie wavelength of the charge carriers becomes comparable to the interparticle distance. Most of modern laboratory and nature plasmas are not sufficiently dense to satisfy this criterion. Some plasmas in space and in a specific laboratory experiments (e.g., plasma X-ray sources) can be relativistic, however for our applications typical plasma temperatures are in the range below 10 keV, so the relativistic effects are not important.

A basic plasma model can be based on classical continuum mechanics using the conservation of mass, momentum and energy. Such a model would involve the equations for basic fluid variables such as average mass density $\rho(\mathbf{x}, t)$, fluid velocity $\mathbf{V}(\mathbf{x}, t)$, energy $T(\mathbf{x}, t)$. The evolution of these macroscopic variables will depend on the position and time. Strictly speaking, plasmas can be well described by fluid equations [1–5], when particle collisions are frequent and the mean free path between particle collisions is short compared to the length scale of the interest (e.g. the wavelength of oscillations) and, as the result, the deviation from a fully thermodynamic state is small. On the other hand, statistical description is applicable and the probability, or distribution function $f(\mathbf{x}, \mathbf{v}, t)$ can be used to characterize the plasma state. The evolution of the distribution function itself is described by the kinetic equation.

Complicated nature of plasma phenomena often makes difficult or impossible the use of an analytical approach, in particular, for a solution of plasma kinetic equations. Therefore, numerical simulations play an important role in a modern plasma physics research. Kinetic

simulations, e.g. particle-in-cell (PIC) methods, or direct solutions of the nonlinear differential kinetic equation, offer comprehensive and the most accurate approach [6–8]. However, such simulations can be very demanding for computational resources (especially in 3D geometries) and can be difficult to interpret. On the other hand, fluid models, based on the evolution of several fluid variables, are generally easier to simulate numerically. They are also easier for physical interpretation.

The problem with the fluid approach, however, is in the absence of kinetic (velocity-dependent) effects which are often critically important for nonlinear plasma dynamics, instabilities and transport, for example, for the ion-temperature-gradient (ITG) driven instabilities [9,10]. Macroscopic plasma variables (density, fluid velocity, pressure,...) can be obtained from the distribution function. The evolution equations for such macroscopic variables are obtained by the integration of the kinetic equation, weighted with increasing powers of the velocity. This procedure results in an infinite hierarchy of moment equations: each of these moment equations involves another variable which is the higher-order moment. Rigorous closure for these equations (higher moments) can be obtained only in the limit of a short mean free path $\lambda \ll L$, and/or strong collisions $\nu \gg \omega$, where ω is the characteristic frequency and L is the characteristic length for the phenomena of interest, $\lambda = v_T/\nu$ is the mean free path between collision, ν is the frequency of collisions, v_T is the particle thermal velocity. In weakly collisional regimes when thermal motion is important these conditions are not satisfied, and one generally needs to refer to the kinetic theory.

One of the important kinetic effects is Landau damping: the collisionless interaction leading to the transfer of energy between the waves and particles. As shown in this work, it is possible to incorporate the linear Landau damping effects into fluid models. A study of Landau-fluid models that include closures for kinetic effects, in particular, for Landau damping, is the goal of this work. The Hammett-Perkins approach [11] using an approximate ansatz was the first systematic approach suggested to address this problem. The derivation of the exact one-dimensional closure for the set of three-moment fluid equations is performed in this thesis with generalized Chapman-Enskog [1] approach. The derived closure exactly reproduces the linear kinetic result and in an appropriate limit reduces to the Hammett-Perkins closure.

The exact linear closure is written in Fourier space and is expressed as a complex function of the mode frequency and the wave number. This means that in nonlinear simulations (that often are performed in configuration space) one needs to perform back and forth transformations between Fourier and configuration space. This is not feasible to do at every time step. A non-Fourier method [12] was suggested recently to avoid this problem [12]. Numerical implementation of the non-Fourier method is another goal of this thesis. I have done this within the plasma fluid simulation framework BOUT++ [13]. In order to verify the numerical implementation, a number of test simulations were performed. These includes evaluation of the plasma response function as well as the self-consistent model for the ion Landau damping. Plasma response function is defined here as plasma density response to the perturbed potential, $\delta n/\delta\phi$, which is prescribed externally with given frequency and the wave number. The plasma response function implemented in BOUT++, both for three- and four-moment fluid models with kinetic closures, shows excellent agreement with the analytical results in Fourier space. In fluid model of the ion sound wave with Landau damping, the potential and the complex wave frequency are determined self-consistently. This self-consistent model shows excellent agreement with the exact linear dispersion relation. Therefore, the simulations verify the numerical implementation of kinetic closures.

The thesis is organized as follows. Introduction starts with general general review of kinetic and fluid plasma equations. Using the example of simple ion sound waves, the limitations of the fluid approach is discussed next: contrary to the kinetic approach, fluid model solution cannot predict the Landau damping. In Chapter **2** it is shown how to overcome this problem by introducing proper kinetic closures for fluid equations. The review of Hammett-Perkins approach [11] is given. Then, I present my derivation of the exact one-dimensional closure with the Chapman-Enskog [1] method for three-moment fluid equations. I show that in a particular limit this result is reduced to the Hammett-Perkins ansatz. I also derive next order corrections to the Hammett-Perkins which give more accurate results. In Chapter **3**, I describe my numerical implementation of the obtained closures and results of my simulations. Appendix **A** reviews of the exact closure models derived in Chang-Callen [14] (CC) and Litt-Smolyakov [15] (LS) works for more general three-dimensional plasma fluid equations. I discuss here some inconsistency between the CC and LS results. Appendix **B** gives

additional information on the plasma dispersion function and its numerical implementation. Appendix C lists some integrals that have been used in the exact linear closures in Chapter 2.

1.1 Plasma models

This section provides a short introduction into the two basic plasma description methods: the microscopic (kinetic) approach and the macroscopic (fluid) approach.

1.1.1 Kinetic plasma equations: Boltzmann and Vlasov models

Since there is a large number of particles in plasmas, it is impractical to describe the coordinates and velocity of each particle. It is conventional to use a distribution function, $f(\mathbf{x}, \mathbf{v}, t)$, to describe the plasma probabilistically. The distribution function gives the number of particles dN per unit volume $d\mathbf{x}d\mathbf{v}$ in a six-dimensional velocity-configuration phase space:

$$f(\mathbf{x}, \mathbf{v}, t) = \frac{dN(\mathbf{x}, \mathbf{v}, t)}{d\mathbf{x}d\mathbf{v}}. \quad (1.1)$$

It can be thought as a number of particles at a given time t in a small phase-space region $\Delta\mathbf{x}\Delta\mathbf{v}$. Due to a large number of particles in real plasmas, the distribution function provides a sufficiently accurate description in a statistical sense. A system of particles can be thought as “fluid” in six-dimensional phase space that evolves in time.

Before introducing the plasma kinetic equations for finding a distribution function in plasma, it is useful to describe some terminology relevant to the distribution function. If the distribution function has coordinate dependence, it is said to be *inhomogeneous*, in contrast to the *homogeneous* case, in which there is no spatial dependence. A dependence on the orientation of the velocity vector \mathbf{v} makes the distribution function *anisotropic*, opposite to the *isotropic* case, when there is no particular direction in the velocity space. Plasma in thermal equilibrium is usually assumed to have a Maxwellian distribution, which is homogeneous, isotropic, and time-independent, given by

$$f_M = \frac{n}{\pi^{3/2}v_T^3} e^{-v^2/v_T^2}, \quad (1.2)$$

where n is the particles number density, $v_T^2 = 2T/m$ is the thermal velocity, and $T \equiv k_B T$ is the temperature, measured in units of energy.

Fig. 1.1 shows several possible types of the Maxwellian distribution in two-dimensional (v_y, v_x) velocity space. It is given in contour plot, i.e. lines of constant value of the function. First, the Maxwellian distribution (1.2) (Fig. 1.1a), represented by concentric circles around zero. Flowing (drifting) Maxwellian (Fig. 1.1b) is the distribution with an average velocity in a particular direction (x -direction in the picture). Anisotropic Maxwellian can arise when a temperature in some direction is different from another, e.g. $T_x > T_y$ (Fig. 1.1c). The so-called bump-on-tail distribution function can arise in a situation when a weak beam is present in the system (Fig. 1.1d) in addition to the Maxwellian for a bulk plasma. The distribution function of the type shown in Fig. 1.1d is an example when in addition to the basic moments of density, pressure and fluid flow velocity, there could be higher-order moments like the heat flux.

Generally the distribution functions need to be defined for each sort of particles in a given system. Therefore, one can define $f_\alpha(\mathbf{x}, \mathbf{v}, t)$, where α corresponds to particle type. To obtain the differential equation for the evolution of the distribution function in space and time, one considers that the number of particles is conserved under the flow in phase space. This conservation law can be written in the form

$$\frac{d}{dt} \int d\mathbf{x} d\mathbf{v} f(\mathbf{x}, \mathbf{v}, t) = 0. \quad (1.3)$$

Together with the conservation of the phase-space volume (Liouville Theorem)

$$\frac{d}{dt} \int d\mathbf{x} d\mathbf{v} = 0, \quad (1.4)$$

it results in the conservation of the distribution function $f_\alpha(\mathbf{x}, \mathbf{v}, t)$ in phase space in the absence of collisions:

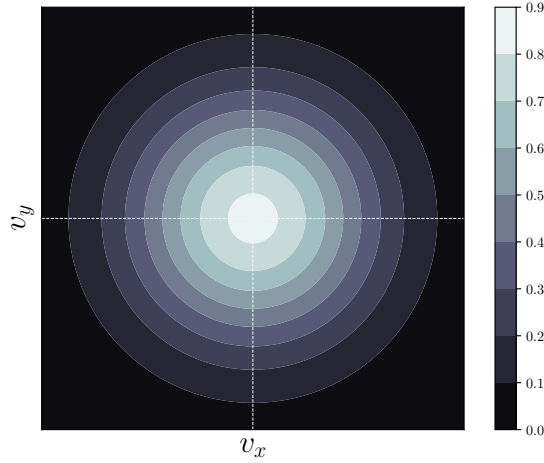
$$\frac{df_\alpha}{dt} = \frac{\partial f_\alpha}{\partial t} + \mathbf{v} \cdot \frac{\partial f_\alpha}{\partial \mathbf{x}} + \mathbf{a} \cdot \frac{\partial f_\alpha}{\partial \mathbf{v}_\alpha} = 0, \quad (1.5)$$

where the chain rule was used to find the total time derivative. Here,

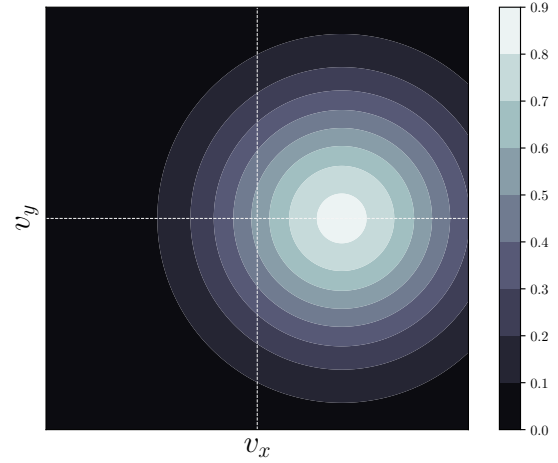
$$\mathbf{v} = \frac{d\mathbf{x}}{dt} \quad (1.6)$$

and

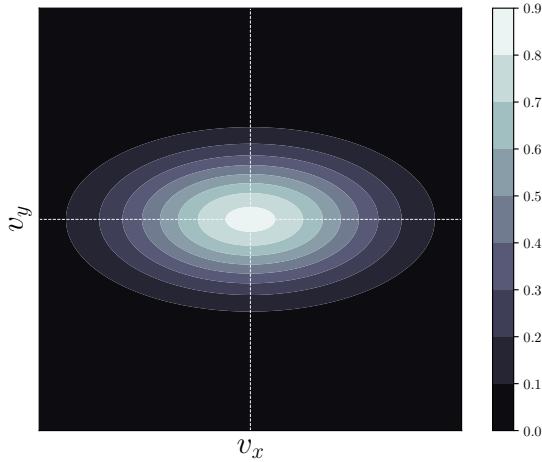
$$\mathbf{a} = \frac{d\mathbf{v}}{dt} \quad (1.7)$$



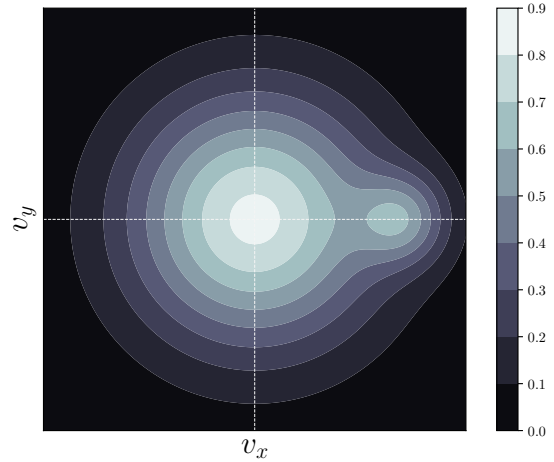
(a) Maxwellian distribution



(b) Flowing Maxwellian



(c) Anisotropic Maxwellian



(d) Bump-on-tail distribution

Figure 1.1: Types of distribution function in 2D (v_x, v_y) phase space, represented with the contour lines of a constant velocity distribution function (arbitrary units). The examples (a), (b), and (c) do not involve the higher-order moments, like the heat flux; (d) is the example of the distribution function with a finite heat flux.

specify the microscopic velocity and acceleration in the phase space. Equations (1.6, 1.7) are equivalent to the characteristics of the PDE in Eq. (1.5). These characteristics are formally written in the form:

$$\frac{d\mathbf{x}}{dt} = \mathbf{v} \quad (1.8)$$

and

$$\frac{d\mathbf{v}}{\frac{q_\alpha}{m_\alpha} \left(\mathbf{E} + \frac{\mathbf{v} \times \mathbf{B}}{c} \right)} = dt. \quad (1.9)$$

Eq. (1.5), describing particle flow in phase space is a collisionless kinetic (Vlasov) equation, or simply Vlasov equation [16]. In plasmas with collisions, the number of particles (in phase space) is not conserved: a particle can be scattered from the given region of velocity space by the collision. It will result in Boltzmann equation:

$$\frac{df_\alpha}{dt} = C(f), \quad (1.10)$$

where $C(f)$ is a collision operator. When the effects caused by particle interactions are negligible, $C(f) = 0$. The present work is focused on collisionless plasma models, therefore the Vlasov equation will be used in our calculations.

Kinetic equation (1.5) can be derived from N-particle distribution function, or Klimontovich equation [17], or from the BBGKY hierarchy [18–22], that provides exact description of many particles in plasma, but are of no direct use due to extremely large number of particles in real systems. Vlasov equation becomes exact when the number of particles in a Debye volume becomes infinite. Strictly speaking, Vlasov equation applies to an ensemble of plasmas, and for a large number of particles in plasma, any fluctuations of the field can be neglected. This is equivalent to replacing the real fields with smoothed (averaged) fields. Including the internal smoothed fields in the force term of Eq. (1.5), one obtains the most known form of Vlasov equation:

$$\frac{\partial f_\alpha}{\partial t} + \mathbf{v} \cdot \frac{\partial f_\alpha}{\partial \mathbf{x}} + \frac{q_\alpha}{m_\alpha} \left(\mathbf{E} + \frac{\mathbf{v}}{c} \times \mathbf{B} \right) \cdot \frac{\partial f_\alpha}{\partial \mathbf{v}} = 0, \quad (1.11)$$

where macroscopic internal electromagnetic fields \mathbf{E} and \mathbf{B} must satisfy Maxwell equations:

$$\operatorname{div} \mathbf{E} = 4\pi\rho, \quad (1.12)$$

$$\operatorname{div} \mathbf{B} = 0, \quad (1.13)$$

$$\operatorname{rot} \mathbf{E} = -\frac{1}{c} \frac{\partial \mathbf{B}}{\partial t}, \quad (1.14)$$

$$\operatorname{rot} \mathbf{B} = \frac{4\pi}{c} \mathbf{J} + \frac{1}{c} \frac{\partial \mathbf{E}}{\partial t}. \quad (1.15)$$

Charge density ρ can be found by summation:

$$\rho(\mathbf{x}, t) = \sum_{\alpha=i,e} q_{\alpha} n_{\alpha}(\mathbf{x}, t), \quad (1.16)$$

where space density n can be found by integrating the distribution function over the entire velocity space:

$$n_{\alpha}(\mathbf{x}, t) = \int_{\mathbf{v}} f_{\alpha}(\mathbf{x}, \mathbf{v}, t) d^3v. \quad (1.17)$$

Current density J is

$$\mathbf{J}(\mathbf{x}, t) = \sum_{\alpha=i,e} q_{\alpha} n_{\alpha}(\mathbf{x}, t) \mathbf{V}(\mathbf{x}, t) = \int_{\mathbf{v}} \mathbf{v} f_{\alpha}(\mathbf{x}, \mathbf{v}, t) d^3v, \quad (1.18)$$

where $\mathbf{V}(\mathbf{x}, t)$ is the average flow velocity. Eqs. (1.11) to (1.18) form a complete set of self-consistent equations to be solved simultaneously and called the Vlasov–Maxwell system. Even though the Vlasov equation (1.5) does not include collision term explicitly, it is not so limited as may appear, as the Lorentz force already includes a number of the effects of particle interactions.

1.1.2 Particle-in-cell method

One of the kinetic methods is to solve Vlasov–Maxwell system (1.11-1.18) by the numerical particle-in-cell (PIC) method. It has been developed and used initially to study hydrodynamic problems [23]. Nowadays, It became the most popular technique for solving kinetic plasma equations numerically. Essentially, PIC is a direct method of following particles along the trajectories in the electric field created by the collection of the same particles. Particles positions are advanced in time in the given electric field, then the field is recalculated at the new positions. The process is then repeated. The information about particle

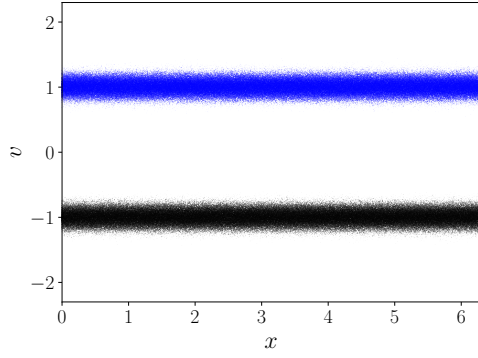
positions and their velocities provides direct knowledge of the particle distribution function. The particles are considered as discrete objects, but for field calculation, charges are spread in space and approximated by the continuous distribution. The field is calculated on the fixed grid (set of cells) and for a continuous distribution of the electric charge, hence the name, particles-in-cell. PIC is relatively simple and straightforward method to implement, though may require significant computational resources for realistic parameters.

For illustrative purposes let us present two examples of PIC simulations which I performed by using the open-source codes [7]. I show here the examples of Landau damping [24] and two-stream instability [25]. Incorporation of the Landau damping into fluid equations is a goal of this work and I show the results of PIC simulations to explain the physics of Landau damping. Landau damping problem is introduced further in this Chapter, along with the analytical approach, and the PIC example is shown at the end of this Chapter. PIC simulations of two-stream instability [26] are used to illustrate the nonlinear regime of wave-particle interactions (nonlinear wave trapping, Fig. 1.2) and discuss the limitations of the linear closures. The PIC calculations can be continued well into the nonlinear stage, and various forms of the distribution functions are observed. Note that the closure methods considered in this work are only good for the linear regime with small deviations, such as in Figs. 1.2a-1.2c. Strong nonlinearity, shown in Figs. 1.2d-1.2f, requires fully nonlinear kinetic approach.

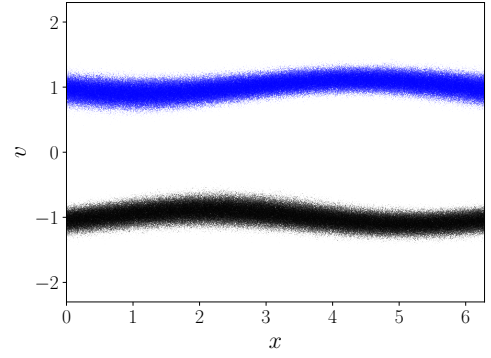
Particle-in-cell simulations for our examples were performed with 1D electrostatic XES1 [27] code, which is a version of the ES1 code (described in [26]) with the support of graphical user interface (X-Window System). ES1 code simulates plasma in a periodic domain, with electrostatic potential solver in Fourier space using Fast-Fourier transform. An integration of equations of motion is done with a popular leap-frog method and Boris scheme for magnetized particles [28].

1.1.3 Fluid plasma equations

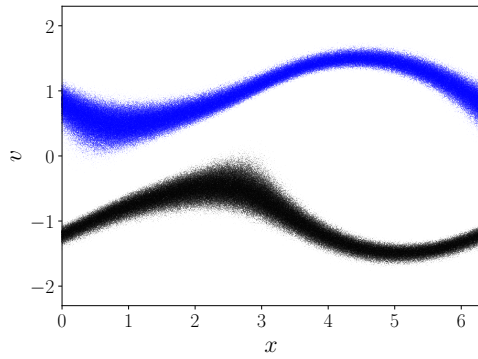
An alternative method of plasma description is based on the fluid model. It describes plasma with the averaged (over a large number of particles) macroscopic variables, such as density, momentum, temperature, and so on. The plasma fluid equations are derived by



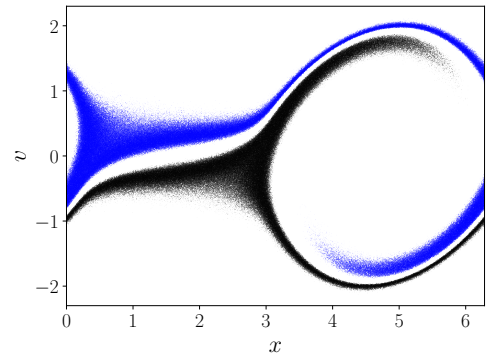
(a) $t\omega_{pe} = 0$



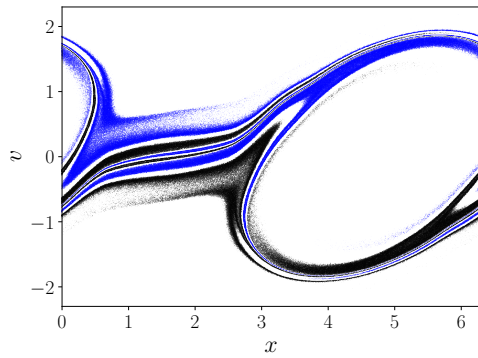
(b) $t\omega_{pe} = 12.4$



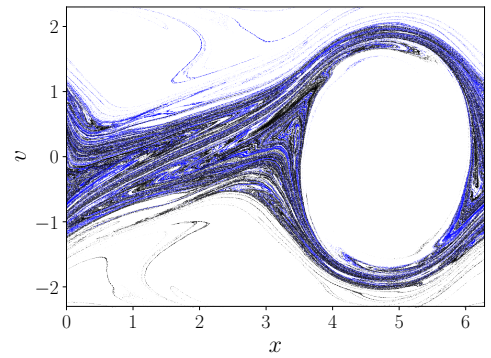
(c) $t\omega_{pe} = 15.8$



(d) $t\omega_{pe} = 18.7$



(e) $t\omega_{pe} = 25.8$



(f) $t\omega_{pe} = 58.4$

Figure 1.2: Phase space evolution for two-stream instability, initialized with the two counter-streaming Maxwellian beams. Beams are represented with black (moving in the negative direction) and blue (moving in the positive direction) dots. System also includes immobile ion's background. Velocity v and coordinate x units are shown in normalized units. Later in the simulation, (d), (e) and (f), the system enters the strongly nonlinear stage with particle trapping and multivalued solutions. These regimes cannot be described by the linear closures studied in this thesis.

taking velocity moments of the Vlasov equation (1.5). This procedure reduces the seven-dimensional space $(\mathbf{x}, \mathbf{v}, t)$ to the four-dimensional space (\mathbf{x}, t) for a finite number of macroscopic fluid variables. The derivation itself can be found in the general plasma physics books [29,30]. It is presented here for the illustrative purpose, to show how the closure problem arises in the system of plasma fluid equations. Let us first represent the kinetic Vlasov equation (1.5) in a conservative form as

$$\frac{\partial f}{\partial t} + \frac{\partial}{\partial \mathbf{x}} \cdot \mathbf{v}f + \frac{\partial}{\partial \mathbf{v}} \cdot \mathbf{a}f = 0, \quad (1.19)$$

where

$$\mathbf{a} = \frac{q}{m} \left(\mathbf{E} + \frac{\mathbf{v}}{c} \times \mathbf{B} \right), \quad (1.20)$$

and indices were omitted for convenience. In the following, the obtained expressions are applicable for ions or electrons. Representation (1.19) is more convenient for the derivation of moment equations. Let us start by taking the first moment by integrating Eq. (1.19) with a moment “1”:

$$\int d^3v \frac{\partial f}{\partial t} + \int d^3v \frac{\partial}{\partial \mathbf{x}} \cdot \mathbf{v}f + \int d^3v \frac{\partial}{\partial \mathbf{v}} \cdot \mathbf{a}f = 0. \quad (1.21)$$

Integrals over the velocity space are taken at constant (t, \mathbf{x}) which allows moving partial derivatives with respect to time and position outside the integrals. This can not be applied to a partial derivative with respect to velocity, but using the divergence theorem one can convert it into a surface integral. Therefore, Eq. (1.21) can be written as

$$\frac{\partial}{\partial t} \int d^3v f + \frac{\partial}{\partial \mathbf{x}} \cdot \int d^3v \mathbf{v}f + \oint_{\infty} d\mathbf{s}_v \cdot \mathbf{a}f = 0. \quad (1.22)$$

By the definition of distribution function, *first term* of (1.22) will give the density moment n . The *second term* of (1.22) is $n\mathbf{V}$, where \mathbf{V} denotes the macroscopic average velocity. Surface integral will result to zero as $\lim_{v \rightarrow \infty} f = 0$. Resulting expression is the density conservation

$$\frac{\partial n}{\partial t} + \nabla \cdot n\mathbf{V} = 0. \quad (1.23)$$

To obtain an equation for momentum evolution, one needs to take the next moment of the Vlasov equation (1.19) by integrating it with a weight $m\mathbf{v}$:

$$m \frac{\partial}{\partial t} \int d^3v \mathbf{v}f + m \frac{\partial}{\partial \mathbf{x}} \cdot \int d^3v \mathbf{v}\mathbf{v}f + m \int d^3v \mathbf{v} \frac{\partial}{\partial \mathbf{v}} \cdot \mathbf{a}f = 0, \quad (1.24)$$

where the *first term* can be immediately written as

$$m \frac{\partial}{\partial t} \int d^3v \mathbf{v} f = m \frac{\partial}{\partial t} (n\mathbf{V}). \quad (1.25)$$

The *second term* of Eq. (1.24) will result in a tensor, as it contains dyadic product $\mathbf{v}\mathbf{v}$. The latter can be simplified by representing the particle velocity as

$$\mathbf{v} = \mathbf{V} + \mathbf{v}', \quad (1.26)$$

where \mathbf{V} is the net fluid velocity and \mathbf{v}' is a random (thermal) velocity, which satisfies $\int d^3v v' f = 0$. It can be written as

$$\mathbf{v}\mathbf{v} = \mathbf{V}\mathbf{V} + \mathbf{V}\mathbf{v}' + \mathbf{v}'\mathbf{V} + \mathbf{v}'\mathbf{v}'. \quad (1.27)$$

The *second term* of Eq. (1.24) can be written as

$$m \frac{\partial}{\partial \mathbf{x}} \cdot \left(\int d^3v \mathbf{V}\mathbf{V} f + \int d^3v \mathbf{v}'\mathbf{v}' f \right) = \nabla \cdot (mn\mathbf{V}\mathbf{V}) + \nabla \cdot \mathbf{\Pi},$$

where $\mathbf{\Pi} = m \int d^3v \mathbf{v}'\mathbf{v}' f$ is a total stress tensor. This tensor can be represented as

$$\mathbf{\Pi} = p\mathbf{I} + \pi, \quad (1.28)$$

where $p = \frac{m}{3} \int d^3v v'^2 f$ is the isotropic pressure, \mathbf{I} - identity tensor, and π is the traceless anisotropic viscosity tensor (or stress tensor), which is defined as

$$\pi = \int d^3v m \left(v'v' - \frac{v'^2}{3} \mathbf{I} \right) f. \quad (1.29)$$

Finally, the *third term* in Eq. (1.24) can be transformed into

$$m \int d^3v \mathbf{v} \frac{\partial}{\partial \mathbf{v}} \cdot \mathbf{a} f = m \int d^3v \left[\frac{\partial}{\partial \mathbf{v}} \cdot \mathbf{v} \mathbf{a} f - \frac{\partial \mathbf{v}}{\partial \mathbf{v}} \cdot \mathbf{a} f \right], \quad (1.30)$$

where the first term goes to zero for the same reasons as before in Eq. (1.22). The last part undergoes the following transformation:

$$m \int d^3v \frac{\partial \mathbf{v}}{\partial \mathbf{v}} \cdot \mathbf{a} f = m \int d^3v \mathbf{I} \cdot \mathbf{a} f = m \int d^3v \mathbf{a} f, \quad (1.31)$$

which results in

$$-mna = -ne \left(\mathbf{E} + \frac{\mathbf{v}}{c} \times \mathbf{B} \right). \quad (1.32)$$

After combining all terms for the second moment (1.24), one has

$$m \frac{\partial}{\partial t} (n \mathbf{V}) + m \nabla \cdot (mn \mathbf{V} \mathbf{V}) + \nabla \cdot \mathbf{\Pi} - ne \left(\mathbf{E} + \frac{\mathbf{v}}{c} \times \mathbf{B} \right) = 0. \quad (1.33)$$

After simplifications and considering the density conservation (1.23) one can write the following momentum conservation equation:

$$mn \frac{D \mathbf{v}}{Dt} = -\nabla p + ne \left(\mathbf{E} + \frac{\mathbf{v}}{c} \times \mathbf{B} \right) - \nabla \pi, \quad (1.34)$$

where the substantial (or total) time derivative operator is:

$$\frac{D}{Dt} \equiv \frac{\partial}{\partial t} + \mathbf{v} \cdot \nabla. \quad (1.35)$$

At this point, the obtained equations for density conservation (1.23) and momentum balance (1.34) are applicable for both electrons and ions. However, this model is not complete: Eq. (1.34) contains the terms with the pressure p and the stress tensor π , which was defined in (1.29). Skipping the full derivation (can be found in [30]) of the pressure moment, the result is

$$\frac{D}{Dt} \left(\frac{3p}{2} \right) + \frac{5p}{2} \nabla \cdot \mathbf{u} = -\mathbf{\Pi} : \nabla \mathbf{u} - \nabla \cdot \mathbf{q}, \quad (1.36)$$

where q is the heat flux, and represent the next (higher order) moment variable, defined as

$$q = \int d^3v f \frac{mv'^2}{2} \mathbf{v}'. \quad (1.37)$$

The derived equations are exact integrals of the collisionless kinetic equation (1.19), presenting particular conservation law, e.g. conservation of particles, momentum, energy, etc. It can also be seen how each of the derived moment equations is coupled together and produce the infinite hierarchy. Therefore, any chosen system of moment equations will not be closed, since each equation involves a higher moment. There are generally two main approaches to the fluid closure problem. One can simply truncate the moment hierarchy, i.e. drop the higher-order moments. This approach was introduced by Grad [31] and has been used in a number of studies of neutral gases [32] and plasmas [33]. Alternatively, one can explicitly calculate (approximately) the higher-order moments from the kinetic theory, as it will be shown in the next section. More accurate perturbation theory approach is based on the Chapman-Enskog method first developed for a neutral gas dominated by collisions [1]. More detailed

description of the approximations resulting in classical transport closures for the fluid plasma equations can be found in Ref. [34]. The description of the Chapman-Enskog method is given in Appendix A for the case of three-dimensional plasma in presence of collisions.

1.1.4 Collisional closures for fluid equations

This section provides the derivation of classical plasma transport coefficients in presence of collisions. These are similar to neutral gases and therefore one can omit the effects of the electric field. The distribution function is considered in the form $f = f_M + \tilde{f}$, where f_M is the Maxwellian distribution (1.2), and \tilde{f} is a small deviation. To solve for distribution function in presence of collisions, one needs the Boltzmann's equation:

$$\frac{\partial f}{\partial t} + \mathbf{v} \cdot \frac{\partial f}{\partial \mathbf{x}} = C(f), \quad (1.38)$$

where the electric field is neglected and $C(f) = -\nu(f - f_M)$ is the Krook's collision operator [29], and f_M is the Maxwellian distribution (1.2). The Krook's operator has a meaning of a relaxation operator resulting in $\tilde{f} = 0$ and thus giving standard Maxwellian distribution, as expected. Considering the stationary case, Eq. (1.38) takes the following form:

$$\mathbf{v} \cdot \frac{\partial f_M}{\partial \mathbf{x}} = -\nu \tilde{f}. \quad (1.39)$$

By allowing the variation in space for density $n(x)$ and temperature $T(x)$ in the Maxwellian distribution, the following gradient for the Maxwellian can be obtained:

$$\frac{\partial f_M}{\partial \mathbf{x}} = \frac{\nabla n}{n} f_M + \frac{\nabla T}{T} \left(-\frac{3}{2} + \frac{v^2}{v_T^2} \right) f_M. \quad (1.40)$$

The perturbed distribution function from Eq. (1.39) is then

$$\tilde{f} = \frac{1}{\nu} \mathbf{v} \cdot \left(\frac{\nabla n}{n} + \frac{\nabla T}{T} \left(-\frac{3}{2} + \frac{v^2}{v_T^2} \right) \right) f_M. \quad (1.41)$$

Using the expression above, one can calculate various macroscopic fluxes by integrating the perturbed distribution function. Such fluxes can be used as closures in the corresponding set of plasma fluid equations. For example, particle flux is defined as

$$\mathbf{\Gamma} = n\mathbf{V} = \int \mathbf{v} \tilde{f} d^3v. \quad (1.42)$$

To obtain the expression for particle flux in the absence of the temperature effects ($T = \text{const}$), one can substitute the expression for \tilde{f} from Eq. (1.41) into Eq. (1.42). It results in the following expression for the particle flux in x -direction:

$$\Gamma_x = -\frac{1}{\nu} \frac{dn}{dx} \frac{1}{n} \int v_x^2 f_M d^3v = \frac{1}{\nu} \frac{dn}{dx} \frac{1}{n} \langle v_x^2 \rangle, \quad (1.43)$$

where averaging is made over Maxwellian distribution. Assuming isotropic velocity space lead to $\langle v_x^2 \rangle = \langle v_y^2 \rangle = \langle v_z^2 \rangle = \langle v^2 \rangle / 3$, therefore only $\langle v^2 \rangle$ can be found. While Maxwellian distribution is isotropic in the velocity space, it is convenient to represent velocity space in spherical coordinates. Integration over the velocity space gives:

$$\int d^3v = \int_0^{2\pi} d\phi \int_0^\pi \sin\theta d\theta \int_0^\infty v^2 dv = 4\pi \int_0^\infty v^2 dv \quad (1.44)$$

The average squared velocity $\langle v^2 \rangle$ can be found in the spherical coordinates representation:

$$\langle v^2 \rangle = \frac{n}{\pi^{3/2} v_T^3} \int_0^\infty 4\pi v^2 e^{-v^2/v_T^2} dv. \quad (1.45)$$

It can be simply evaluated with integration by parts and results into $\langle v^2 \rangle = \frac{3}{2} n v_T^2$. Therefore, particle flux $\mathbf{\Gamma}$ due to the gradient in density is

$$\mathbf{\Gamma} = -D_\nu \nabla n, \quad (1.46)$$

where $D_\nu = \frac{v_T^2}{2\nu}$. This expression is also known as the Fick's first law [35]. The expression for the particle flux can be interpreted as the closure for the continuity equation: no additional equations are needed to describe the evolution of the density. Substituting the obtained particle flux (1.46) into the continuity equation (1.23), the diffusion equation for the density (or Fick's second law) is obtained:

$$\frac{\partial n}{\partial t} = D_\nu \nabla^2 n. \quad (1.47)$$

Next, one can derive an expression for collisional heat flux q , which is defined as

$$q = \frac{m}{2} \int \mathbf{v}^2 \mathbf{v} \tilde{f} d^3v. \quad (1.48)$$

With $n = \text{const}$ in Eq. (1.41), the heat flux in x -direction is

$$q_x = -\frac{m}{2} \frac{1}{\nu} \frac{dT}{dx} \frac{1}{T} \int v^2 v_x^2 \left(-\frac{3}{2} - \frac{v^2}{v_T^2} \right) f_M d^3v. \quad (1.49)$$

Two integrals should be evaluated, $\langle v^2 v_x^2 \rangle$ and $\langle v^4 v_x^2 \rangle$. Again, by the assumption of isotropic velocity space, $\langle v^2 v_x^2 \rangle = \langle v^2 v_z^2 \rangle$. Using spherical coordinates representation (1.44), one can find

$$\langle v^2 v_z^2 \rangle = \int_0^{2\pi} d\phi \int_0^\pi \cos^2 \theta \sin \theta d\theta \int_0^\infty v^6 f_M dv = \frac{4}{3} \pi \int_0^\infty v^6 f_M dv, \quad (1.50)$$

$$\langle v^4 v_z^2 \rangle = \frac{4}{3} \pi \int_0^\infty v^8 f_M dv. \quad (1.51)$$

Both integrals can be evaluated with integration by parts, and the heat flux results in

$$q = -D_T n \nabla T, \quad (1.52)$$

where $D_T = \frac{5v_T^2}{2\nu}$.

To evaluate the momentum diffusion (stress tensor) $\mathbf{\Pi}$ (and a viscous force, associated with it), one needs to assume a moving Maxwellian:

$$f_M(\mathbf{x}, v) = \frac{n}{\pi^{3/2} v_T^3} \exp\left(-\frac{(v - V(\mathbf{x}))^2}{v_T^2}\right), \quad (1.53)$$

where $n = \text{const}$, $T = \text{const}$, and $V(\mathbf{x})$ is the fluid velocity. Then, dropping nonlinear terms, one can show that

$$\mathbf{v} \cdot \nabla f_M = -\frac{f_M}{v_T^2} v_\alpha v_\beta \left(\frac{\partial V_\beta}{\partial x_\alpha} + \frac{\partial V_\alpha}{\partial x_\beta} \right). \quad (1.54)$$

By the assumption of the shear plane-parallel flow $\mathbf{V} = V_y(x) \hat{\mathbf{e}}_y$, where $\hat{\mathbf{e}}_y$ is the unit vector in y -direction, the momentum diffusion tensor can be obtained as

$$\Pi_{xy} = m \int v_x v_y \tilde{f} d^3 v = -m \frac{1}{\nu} \frac{1}{v_T^2} \frac{\partial V_y}{\partial x} \int v_x^2 v_y^2 f_M d^3 v, \quad (1.55)$$

which requires to evaluate $\langle v_x^2 v_y^2 \rangle$, which results in the integral:

$$\langle v_x^2 v_y^2 \rangle = \frac{n}{v_T^3 \pi^{3/2}} \int_0^{2\pi} \cos^2 \phi \sin^2 \phi d\phi \int_0^\pi \sin^5 \theta d\theta \int_0^\infty v^6 e^{-v^2/v_T^2} dv, \quad (1.56)$$

which results in $\langle v_x^2 v_y^2 \rangle = n v_T^4 / 4$. Substituting it into Eq. (1.55), one gets

$$\Pi_{xy} = -\frac{v_T^2}{m\nu} n m \frac{\partial V_y}{\partial x}. \quad (1.57)$$

Finally, the viscous force, defined as $\mathbf{F} \equiv \nabla \cdot \Pi$, can be found in y -direction:

$$F_y = -D_\nu mn \frac{\partial V_y^2}{\partial x^2}, \quad (1.58)$$

where $D_\nu = \frac{v_T^2}{2\nu}$.

All three diffusion coefficients have a similar scaling $D \sim v_T^2/\nu$, which is consistent with the random-walk diffusion model. The random-walk processes are characterized by $D \sim (\Delta x)^2/\tau$, where Δx is the average displacement in time τ before particle changes its direction (e.g., collide). Thus, for plasma Δx has a meaning of the free path, with τ as a time between collisions. Then $D \sim v_T^2/\nu$, where $\nu \sim 1/\tau$ and $v_T = \Delta x/\tau$.

The method discussed above allows to estimate the main transport coefficients in the presence of collisions. For a more accurate result, one can use a general Chapman-Enskog method described in Appendix A.

1.2 Waves in plasmas

In this section both kinetic and fluid models will be used to describe ion sound waves in plasmas. The advantage of fluid model is simplicity: equations are solved in three spatial dimensions and time instead of the six-dimensional phase space and time for the kinetic, e.g. Vlasov equation. The disadvantage of the fluid approach, however, is the absence of the particle thermal effects such as Landau damping.

1.2.1 Ion sound waves

Ion sound waves are longitudinal oscillations of plasma density and electric field (wave of rarefaction and compression). They are similar to ordinary sound waves in neutral gases with the main difference in that the ion sound waves are supported in collisionless plasma by long distance electrostatic interactions. This interaction is mediated by the electrons which due to their small mass follow the potential trying to keep the quasineutrality.

The plasma is assumed to consist of a single species of ions and electrons. Equations of continuity (1.23) and momentum (1.34) in a one-dimensional case are:

$$\frac{\partial n_\alpha}{\partial t} + \frac{\partial}{\partial z} (v_\alpha n_\alpha) = 0, \quad (1.59a)$$

$$m_\alpha n_\alpha \left(\frac{\partial}{\partial t} + v_\alpha \frac{\partial}{\partial z} \right) v_\alpha = -\frac{\partial p_\alpha}{\partial z} - q_\alpha n_\alpha \frac{\partial \phi}{\partial z}, \quad (1.59b)$$

where α is species type index (e or i). Here n, v, p, ϕ are the particle density, velocity, pressure and electrostatic potential, respectively. No external electric or magnetic field is assumed. The self-consistent electric potential is found from the Poisson equation

$$\frac{\partial^2 \phi}{\partial z^2} = -4\pi \sum_\alpha e_\alpha n_\alpha. \quad (1.60)$$

The ion temperature for this problem is considered to be much smaller than that of electrons, $T_i \ll T_e$. As it will be shown with kinetic theory, in the case of $T_i \sim T_e$ ion sound waves would be greatly affected (usually damped) by Landau damping. By letting $T_i = 0$ for ions one obtains:

$$\frac{\partial n_i}{\partial t} + \frac{\partial}{\partial z} (v_i n_i) = 0, \quad (1.61a)$$

$$m_i n_i \left(\frac{\partial}{\partial t} + v_i \frac{\partial}{\partial z} \right) v_i = -en_i \frac{\partial \phi}{\partial z}. \quad (1.61b)$$

Since the wave frequency for sound waves ω is small compared to the plasma frequency ω_{pe} , and the ions are much heavier than electrons, one can neglect electron mass in the momentum balance equation for electrons, which will result in

$$-\nabla p_e + en_e \nabla \phi = 0. \quad (1.62)$$

In the limit $\omega \ll kv_{Te}$, the perturbations of the electron temperature are small and one assumes $T_e = \text{const}$, which gives

$$\frac{\nabla n_e}{n_e} = \frac{e}{T_e} \nabla \phi. \quad (1.63)$$

By integrating this equation, one obtains the Boltzmann equation for electrons

$$n_e = n_{0e} \exp\left(\frac{e\phi}{T_e}\right), \quad (1.64)$$

which effectively shows the ‘‘immediate’’ electron response related to changes in potential. Here n_{0e} is the equilibrium electron density.

Let us consider linear wave oscillations with small deviations from stationary equilibrium state. Therefore, all variables can be expanded around the equilibrium:

$$X(x, t) = X_0(x) + \tilde{X}(x, t), \quad (1.65)$$

where $X_0(x)$ is the equilibrium state and $\tilde{X}(x, t)$ is a linear perturbation, $\tilde{X} \ll X_0$. Linearizing Eqs. (1.60), (1.61), (1.64) and assuming $n_{0e} = n_{0i} = n_0$, the full system of equations is: (tilde sign for perturbed values is omitted and isotropic equilibrium state assumed)

$$\frac{\partial n_i}{\partial t} + n_0 \frac{\partial v_i}{\partial z} = 0, \quad (1.66a)$$

$$m_i \frac{\partial v_i}{\partial t} + e \frac{\partial \phi}{\partial z} = 0, \quad (1.66b)$$

$$n_e = n_0 \frac{e\phi}{T_e}, \quad (1.66c)$$

$$\frac{\partial^2 \phi}{\partial z^2} = -4\pi e (n_i - n_e), \quad (1.66d)$$

where n_i, v_i, ϕ are small deviations from equilibrium values.

Assuming a quasi-neutral approximation $n_i = n_e$ in Eqs. (1.66) and looking for a solution in the form $X \sim e^{-i(\omega t - kz)}$, the dispersion relation is

$$\omega^2 = c_s^2 k^2, \quad (1.67)$$

where $c_s^2 = T_e/m_i$ is the ion sound velocity. Replacing quasi-neutrality condition with Poisson equation (1.66d) will result in the dispersion equation

$$\omega^2 = \frac{c_s^2 k^2}{1 + k^2 \lambda_D^2}, \quad (1.68)$$

where $\lambda_D^2 = T_e/(4\pi n_0 e^2)$ - Debye length. The Eq. (1.68) includes the dispersion of the ion sound waves, and in short wavelength regime $k^2 \lambda_D^2 \gg 1$ the frequency is bound from above by the ion plasma frequency $\omega_{pi} = \sqrt{4\pi n e^2/m_i}$.

1.2.2 Electrostatic waves in kinetic theory and ion Landau damping

In this section, the linear dispersion relation for the ion acoustic waves will be derived by using the kinetic approach. As in the previous section, the one-dimensional model will be be

investigated here. To start, one needs one-dimensional Vlasov equation in the absence of the magnetic field:

$$\frac{\partial f_\alpha}{\partial t} + v \frac{\partial f_\alpha}{\partial x} + \frac{q_\alpha}{m_\alpha} E \frac{\partial f_\alpha}{\partial v} = 0. \quad (1.69)$$

Further, a perturbed distribution function in the form $f_\alpha(x, v, t) = f_{0\alpha}(v) + f_{1\alpha}(x, v, t)$ is assumed. Seeking a solution in the form of $f_{1\alpha} \sim e^{-i(\omega t - kx)}$, the first order term $f_{1\alpha}$ is found from Eq. (1.69) in Fourier space:

$$f_{1\alpha} = \frac{q_\alpha k \phi}{m_\alpha} \frac{\partial f_{0\alpha} / \partial v}{\omega - kv}, \quad (1.70)$$

where ϕ is the perturbed potential. Note that Eq. (1.70) contains singularity at $\omega = kv$ due to the particle-wave resonant interaction. From the perturbed distribution function, the density perturbation can be found by integrating over the velocity space:

$$n_{1\alpha} = \frac{n_{0\alpha} q_\alpha k \phi}{m_\alpha} \int_{-\infty}^{\infty} \frac{\partial f_{0\alpha} / \partial v}{\omega - kv} dv, \quad (1.71)$$

and after substitution it to the Poisson equation (1.60), one obtains the general dispersion relation:

$$1 + \sum_{\alpha} \frac{\omega_{p\alpha}^2}{k^2} \int_{-\infty}^{\infty} \frac{\partial f_{0\alpha} / \partial v}{v - \omega/k} dv = 0, \quad (1.72)$$

where $\omega_{p\alpha} = \sqrt{(4\pi n_{0\alpha} q_\alpha^2) / m_\alpha}$ is the plasma frequency (for α species).

The obtained dispersion relation contains the singularity at $\omega = kv$, and the first approach to handle it is to take the principal value of the integral, as done by Vlasov [36]. The singular part of the integrand $1/(v - \omega/k)$ is eliminated via the principal value integration, i.e.

$$\text{P.V.} \int_{-\infty}^{\infty} \frac{dv}{v - \omega/k} = \lim_{\epsilon \rightarrow 0} \left[\int_{-\infty}^{\omega/k - \epsilon} \frac{dv}{v - \omega/k} + \int_{\omega/k + \epsilon}^{\infty} \frac{dv}{v - \omega/k} \right], \quad (1.73)$$

giving a real and finite value. Landau showed [24] that the correct way to treat the problem is through an initial value problem, which requires to perform the Laplace transform in time. Then the dispersion relation takes the form which has an additional imaginary term: (for a cold plasma limit $\omega/k \gg v$)

$$1 + \sum_{\alpha} \frac{\omega_{p\alpha}^2}{k^2} \left[\int_{-\infty}^{\infty} \frac{\partial f_{0\alpha} / \partial v}{v - \omega/k} dv + i\pi \frac{\partial f_{0\alpha}}{\partial v} \Big|_{v=\omega/k} \right] = 0. \quad (1.74)$$

One can use another approach to represent the general kinetic dispersion relation, with the help of a plasma dispersion function $Z(\zeta)$ [37], defined as

$$Z(\zeta) = \frac{1}{\pi^{1/2}} \int_{-\infty}^{\infty} \frac{e^{-s^2}}{s - \zeta} ds, \quad \text{Im } \zeta > 0. \quad (1.75)$$

Useful property can be noted that if to differentiate $Z(\zeta)$ with respect to ζ , one can obtain

$$Z'(\zeta) = \frac{-1}{\pi^{1/2}} \int_{-\infty}^{\infty} \frac{2s}{s - \zeta} e^{-s^2} ds, \quad (1.76)$$

which yields via the integration by parts

$$Z'(\zeta) = -2(1 + \zeta Z). \quad (1.77)$$

It will be shown shortly that $\zeta = \omega/(kv_T)$ is the normalized frequency in our application. It is useful to present two limiting cases of the plasma dispersion function $Z(\zeta)$, adiabatic (particles moves faster compared to the wave phase velocity), $\zeta \ll 1$:

$$Z(\zeta) = i\pi^{1/2}e^{-\zeta^2} - 2\zeta + \frac{4\zeta^3}{3} - \frac{8\zeta^5}{15} + \dots, \quad (1.78)$$

and fluid limit, with $\zeta \gg 1$,

$$Z(\zeta) = i\pi^{1/2}\sigma e^{-\zeta^2} - \frac{1}{\zeta} - \frac{1}{2\zeta^3} - \frac{3}{4\zeta^5} + \dots, \quad (1.79)$$

where

$$\sigma = \begin{cases} 0, & \text{Im } \zeta > 0, \\ 1, & \text{Im } \zeta = 0, \\ 2, & \text{Im } \zeta < 0. \end{cases} \quad (1.80)$$

It is also convenient to introduce the plasma response function $R(\zeta)$, given by

$$R(\zeta) = 1 + \zeta Z(\zeta). \quad (1.81)$$

For a small argument (adiabatic) approximation $\zeta \ll 1$ gives

$$R(\zeta) \approx 1 + i\sqrt{\pi}\zeta e^{-\zeta^2} - 2\zeta^2 + \frac{4}{3}\zeta^4, \quad (1.82)$$

and asymptotic expansion for the fluid case with large $\zeta \gg 1$:

$$R(\zeta) \approx i\sqrt{\pi}\zeta\sigma e^{-\zeta^2} - \frac{1}{2\zeta^2} - \frac{3}{4\zeta^4}, \quad (1.83)$$

where σ is given above (1.80).

To take the advantage of special functions being introduced, one can transform Eq. (1.71), assuming that $f_{0\alpha}$ is Maxwellian, into

$$n_{1\alpha} = \frac{q_\alpha \phi n_{0\alpha}}{m_\alpha v_{T\alpha}} \int_{-\infty}^{\infty} \frac{(d/ds)(e^{-s^2})}{s - \zeta_\alpha} ds, \quad (1.84)$$

where $\zeta_\alpha = \omega/(kv_{T\alpha})$. This allows to represent density perturbation with the plasma response function:

$$n_{1\alpha} = R_\alpha(\zeta_\alpha) \frac{q_\alpha \phi}{T_\alpha} n_{0\alpha}. \quad (1.85)$$

Finally, to obtain general dispersion relation for one-dimensional longitudinal (electrostatic) waves, one needs to substitute the density perturbation (1.85) into use Poisson equation (1.60):

$$-1 = \frac{1}{k^2 \lambda_D^2} R(\zeta_e) + \frac{2\omega_{pi}^2}{k^2 v_{Ti}^2} R(\zeta_i). \quad (1.86)$$

The basic longitudinal modes are high-frequency electron plasma oscillations (and related electron plasma waves with finite electron temperature) and low-frequency ion sound waves. For high-frequency electron oscillations, the effect of heavy ions can be neglected, thus imposing $\omega_{pi}^2 = 0$. For cold electrons, $\zeta_e \gg 1$ and the corresponding asymptotic expansion leads to $R_e = -k^2 v_{Te}^2 / 2\omega^2$. Thus, from Eq. (1.86) one gets $\omega^2 = \omega_{pe}^2$. Keeping the small corrections due to electron temperature, one obtains:

$$R_e = -\frac{k^2 v_{Te}^2}{2\omega^2} - \frac{3}{4} \left(\frac{k^2 v_{Te}^2}{\omega^2} \right)^2, \quad (1.87)$$

and from Eq. (1.86) the Langmuir (or Bohm-Gross) waves can be found:

$$\omega^2 = \omega_{pe}^2 + 3k^2 v_{Te}^2, \quad (1.88)$$

where the approximation $\omega^2 \simeq \omega_{pe}^2$ have been used in the second term of Eq. (1.87). The ion sound waves are low-frequency waves in the range $kv_{Ti} \ll \omega \ll kv_{Te}$, which implies $\zeta_e \ll 1$ and $\zeta_i \gg 1$. The electron Landau damping can be neglected for the ion sound waves because the slope of $f_e(v)$ is small near its peak. For electrons, the condition $\zeta_e \ll 1$ corresponds to the Boltzmann density $n_e = n_0 e \phi / T_e$ and response function $R_e \approx 1$. For $k^2 \lambda_D^2 \ll 1$ one obtains the dispersion relation from Eq. (1.86):

$$R(\zeta) = -\tau, \quad (1.89)$$

where $\tau \equiv T_{0i}/T_{0e}$. To solve this equation, one can assume complex ω and real k , while seeking a damping rate of the initially placed wave. Therefore roots must satisfy $\text{Re}(\mathbf{R}) = \tau$, $\text{Im}(\mathbf{R}) = 0$. This problem can be treated as the system of two nonlinear equations of two arguments (complex plane). This is illustrated in Fig. 1.3, where the contour plots for each of the equations are given on the complex plane. Roots can be found in the intersection points. From all possible roots with $\text{Im } \omega < 0$, the dominant root is the one having the smallest $|\text{Im } \omega|$. The exact numerical solution of Eq. (1.89) presented in Fig. 1.4.

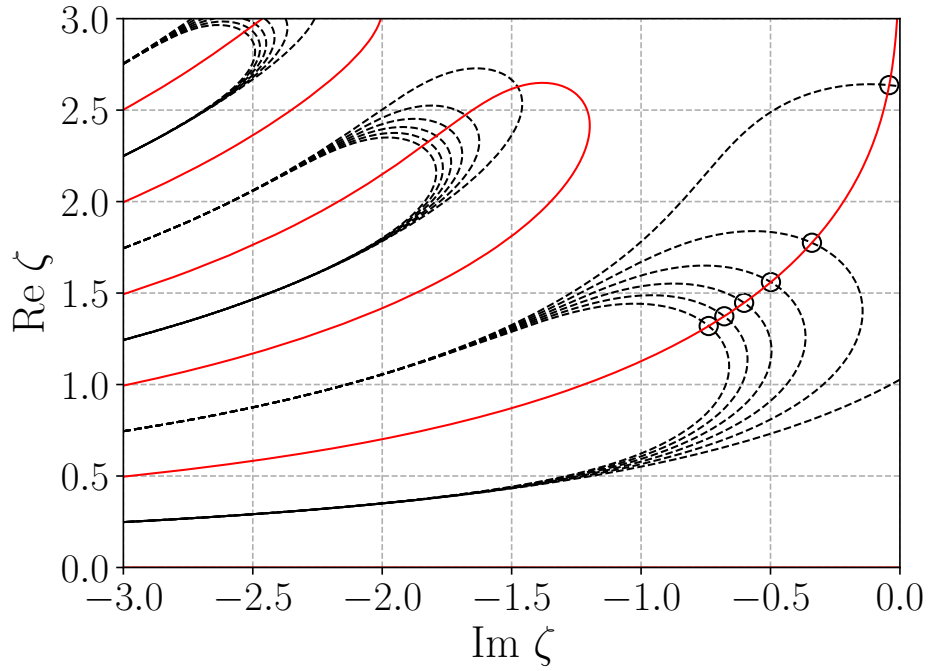


Figure 1.3: Complex plane with contour lines of $\text{Im}(\mathbf{R}) = 0$ (red) and $\text{Re}(\mathbf{R}) = -\tau$ (black) for values of $\tau = 0.1, 0.4, 0.7, 1.0, 1.3, 1.6$. Roots with the smallest $|\text{Im } \omega|$ are circled.

To obtain an approximate solution, one needs to use the limiting cases of the plasma response function. Taking the first two real terms for ions from (1.83)

$$\mathbf{R}_i \approx -\frac{1}{2} \frac{k^2 v_{Ti}^2}{\omega^2} - \frac{3}{4} \frac{k^4 v_{Ti}^4}{\omega^4}, \quad (1.90)$$

and substituting it into Eq. (1.86), one can obtain the ion sound dispersion relation:

$$\omega^2 = \frac{k^2 c_s^2}{1 + k^2 \lambda_D^2}, \quad (1.91)$$

which is equivalent to the result (1.68) that obtained by using two-moment fluid approximation. But Eq. (1.83) contains also the imaginary term, responsible for the Landau damping. By including it into the ion response function $R(\zeta_i)$, the resulted dispersion relation is given by

$$-1 = \frac{1}{k^2 \lambda_D^2} + \frac{2\omega_{pi}^2}{k^2 v_{Ti}^2} \left(i\sqrt{\pi}\zeta_i e^{-\zeta_i^2} - \frac{1}{2\zeta_i^2} - \frac{3}{4\zeta_i^4} \right). \quad (1.92)$$

In a first approximation the Landau damping term can be neglected:

$$\frac{1}{\tau} \left(-\frac{1}{2\zeta_i^2} - \frac{3}{4\zeta_i^4} \right) = -1 - k^2 \lambda_D^2 \simeq -1, \quad (1.93)$$

where term $k^2 \lambda_D^2$ is also neglected, assuming weak dispersion case. Thus,

$$\frac{1}{\zeta_i^2} \left(1 + \frac{3}{2\zeta_i^2} \right) = 2\tau. \quad (1.94)$$

While $\zeta_i \gg 1$, the approximation $1/\zeta_i^2 \approx 2\tau$ can be substituted into the previous equation to obtain

$$\zeta_i^2 = \frac{1 + 3\tau}{2\tau}, \quad (1.95)$$

or

$$\frac{\omega^2}{k^2} = \frac{T_e + 3T_i}{m_i}, \quad (1.96)$$

which is the standard dispersion relation for the ion acoustic waves. With this one can handle the imaginary term of Eq. (1.92):

$$-i\sqrt{\pi}\zeta_i e^{-\zeta_i^2} + \frac{1}{2\zeta_i^2} + \frac{3}{4\zeta_i^4} = \tau, \quad (1.97)$$

$$-2i\sqrt{\pi}\zeta_i e^{-\zeta_i^2} + \frac{1}{\zeta_i^2} \left(1 + \frac{3}{2\zeta_i^2} \right) = 2\tau, \quad (1.98)$$

and substitute $1/\zeta_i^2 \approx 2\tau$:

$$\zeta_i = \left(\frac{1 + 3\tau}{2\tau} \right)^{1/2} \left(1 + i\frac{1}{\tau}\sqrt{\pi}\zeta_i e^{-\zeta_i^2} \right)^{-1/2}. \quad (1.99)$$

Finally, expanding the square root, the approximate solution is

$$\zeta_i \approx \left(\frac{1 + 3\tau}{2\tau} \right)^{1/2} \left(1 - \frac{i}{2\tau}\sqrt{\pi}\zeta_i e^{-\zeta_i^2} \right), \quad (1.100)$$

resulting in approximate damping rate

$$-\frac{\text{Im } \zeta_i}{\text{Re } \zeta_i} = \sqrt{\frac{\pi}{8}} \sqrt{\frac{1+3\tau}{\tau^3}} e^{-(1+3\tau)/(2\tau)}, \quad (1.101)$$

where the Eq. (1.95) is used for the ζ_i in the imaginary part. The negative imaginary part of the obtained wave frequency implies damping in time. It can be shown with a wave in the form $X \sim e^{-i\omega t}$, where complex negative frequency $\omega = -i\gamma$; then $X \sim e^{-\gamma t}$. Therefore, $\text{Im } \omega$ represents a damping rate, which usually is being noted as γ . Resulted approximate solution for the ion Landau damping (1.101) is plotted in Fig. 1.4, along with the exact (numerical) solution of Eq. (1.89).

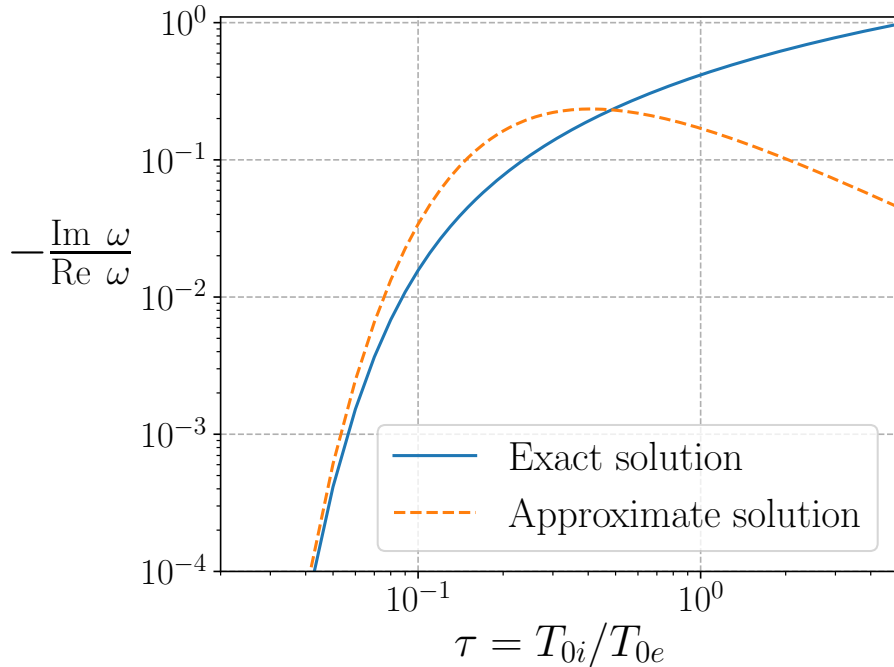


Figure 1.4: Landau damping for ion sound waves. Exact solution of Eq. (1.89) represented with solid line, approximate solution (1.101) with a dashed line.

To illustrate the effects, related to Landau damping, a one-dimensional particle-in-cell (PIC) simulation is presented. The initial electrostatic wave is considered which is damped due to finite electron temperature. The ions are heavy and immobile. The kinetic dispersion relation is solved for the damping rate and compared with PIC results. By neglecting the

ion dynamics $\omega_{pi} = 0$ in Eq. (1.86) one has

$$-1 = \frac{1}{k^2 \lambda_D^2} \text{R}(\zeta_e). \quad (1.102)$$

Seeking an electron plasma oscillations, $\omega/k \gg v_{Te}$, the plasma response function (1.83) for the large argument approximation can be written as

$$-1 = \frac{1}{k^2 \lambda_D^2} \left(2i\sqrt{\pi}\zeta e^{-\zeta^2} \frac{1}{2\zeta^2} \right), \quad (1.103)$$

from where one finds ζ :

$$\zeta = \left(\frac{1}{2k^2 \lambda_D^2} - 2i\sqrt{\pi} \frac{1}{2k^2 \lambda_D^2} \zeta e^{-\zeta^2} \right)^{1/2}. \quad (1.104)$$

Expansion of the square root (assuming small imaginary term) gives the result

$$\text{Im } \omega \approx -e^{-3/2} \sqrt{\pi} \frac{\omega_{pe}}{(2k^2 \lambda_D^2)^{3/2}} e^{-1/(2k^2 \lambda_D^2)}, \quad (1.105)$$

where the real part of plasma waves $\omega^2 = \omega_{pe}^2 + 3k^2 v_{Te}^2$ was used in the imaginary part. For $k\lambda_D = 0.5$ Eq. (1.105) provides the damping rate $\text{Im } \omega = -0.154 \omega_{pe}$.

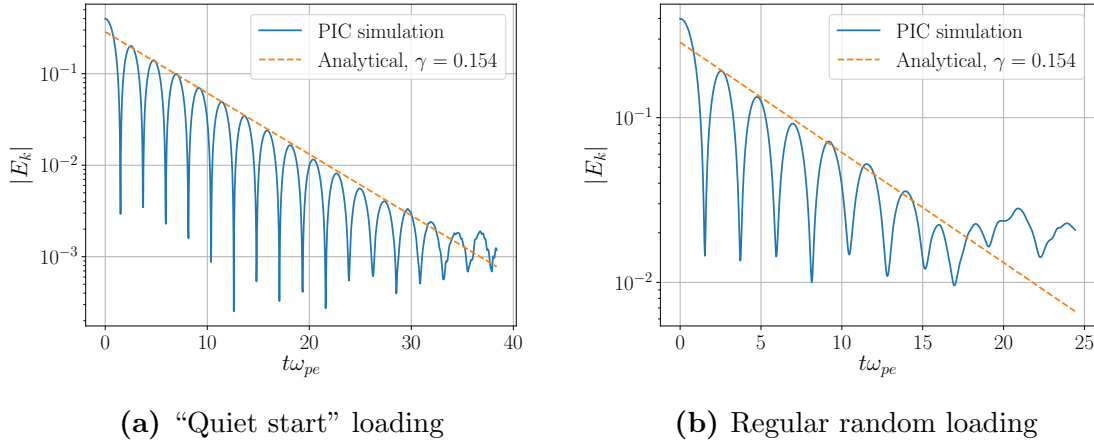


Figure 1.5: Landau damping of an electrostatic wave for two different initial distributions: (a) “quiet start” with a well represented Maxwellian; (b) random Maxwellian distribution.

For this simulation, let us assume the initial perturbation of the electron density $n_e \sim \sin(k_0 x)$ with $k_0 \lambda_D = 0.5$. The Landau damping effect strongly depends on the velocity distribution function (VDF) representation. In fact, as shown in Fig. 1.5, a better representation for the VDF results in greater damping. The so-called “quiet start” technique

initializes particles uniformly in space with a non-random Maxwellian VDF [6]. The difference between the distribution functions from quiet start and regular particle loading is represented in Fig. 1.6. Quiet start loading results in wave damping, consistent with the analytical result (Fig. 1.5a). As reported previously [6], the Landau damping was observed only with the quiet start technique, however only $\sim 2^6$ macroparticles per cell had been used. Loading more particles, $\sim 2^{11}$ per cell results in Landau damping (Fig. 1.5b) with a regular loading of particles. Obviously, larger number of particles reduce the noise in the VDF initialization.

Fig. 1.7 demonstrates the collisionless dissipation mechanism of Landau damping, in which the energy transfers from the wave to the particles. The electrostatic wave energy $\int dx E(x)^2 / (8\pi)$ is transferred to the kinetic energy of electrons $\sum_{i=1}^N m_e v_i^2 / 2$ resulting the wave damping.

Finally, the phase space mixing during the Landau damping can be seen in Fig. 1.8. This mixing starts in the region $\omega/k \approx v_{Te}$, where resonance occurs between particles and a wave.

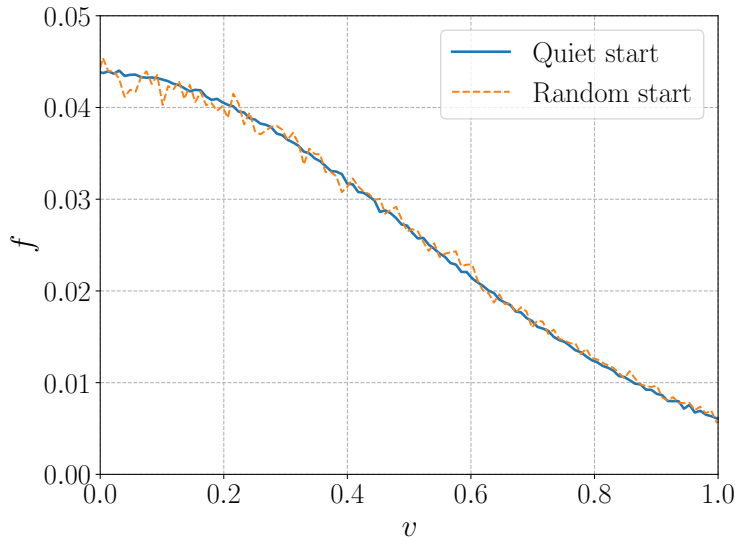


Figure 1.6: Velocity distribution function produced with two methods of initial particle loading in the XES1 code: quiet start technique (solid) and random particle distribution (dashed).

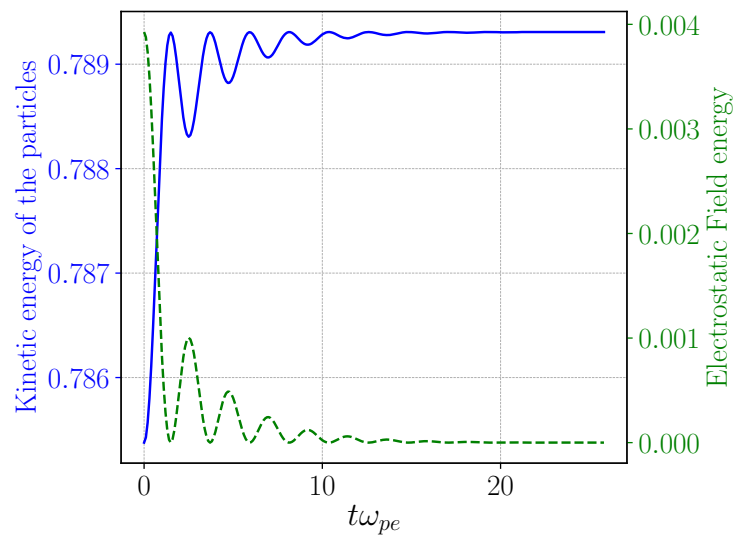
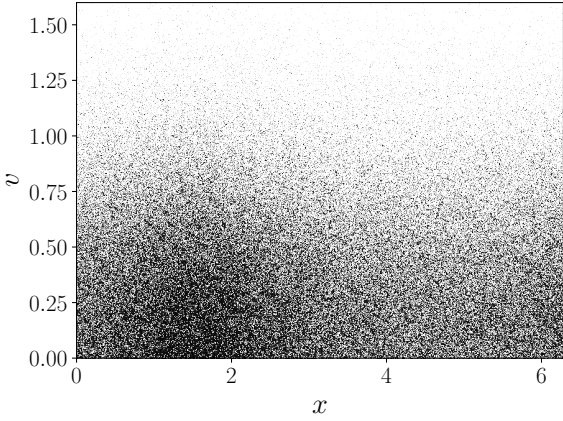
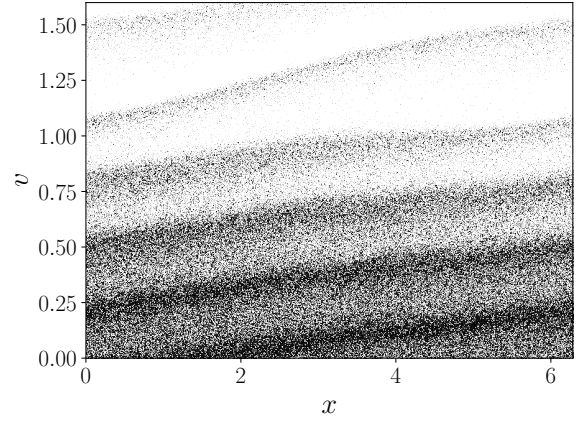


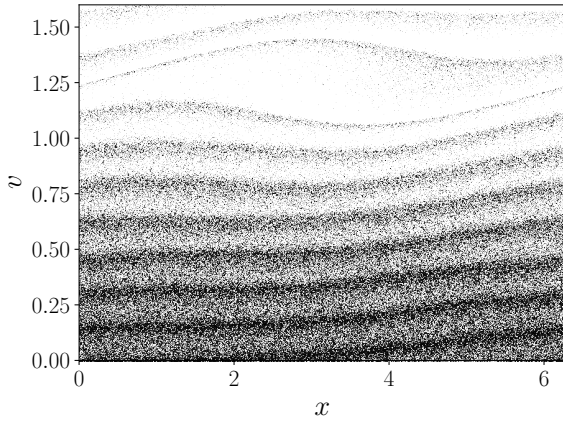
Figure 1.7: Conservation of energy in the simulation of Landau damping. Energy from the initial electrostatic wave (dashed line) has been transferred to particles kinetic energy (solid line). Energy units are normalized.



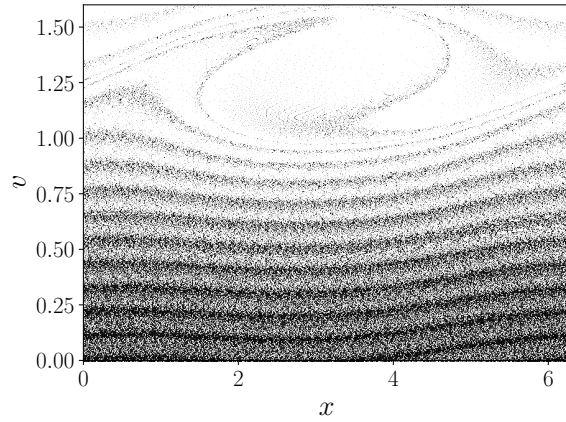
(a) $t\omega_{pe} = 0$



(b) $t\omega_{pe} = 20.15$



(c) $t\omega_{pe} = 38.6$



(d) $t\omega_{pe} = 58.4$

Figure 1.8: Phase-space evolution of the electron component of the plasma during the Landau damping simulation. Due to symmetry, only the positive velocity region plotted. Linear regime is characterized by shearing of the initial perturbation (b), in nonlinear regime particle trapping occurs (holes in phase space) which stops damping, (c)-(d). The linear closures are not valid in strongly nonlinear regimes.

CHAPTER 2

ONE-DIMENSIONAL COLLISIONLESS CLOSURES

Fluid equations provide an adequate description of many problems. In contrast to the kinetic approach, they are generally more amenable to analytic insights and numerical simulations. Their reduced dimensionality provides simpler physical interpretation and lowers computational cost compared to the fully kinetic approach. In general, however, wave-particle interactions (Landau damping) are not captured by fluid models. Some kinetic effects can be included in fluid equations via linear closures [38]. Hammett and Perkins (HP) [11] were the first to propose some systematic approach to this problem. They suggested an approximate closure, based on the ad-hoc matching of a “reasonable” expression with the exact kinetic result (for the plasma response function). This Chapter starts with a more detailed description of the HP approach. Then it is shown, that in fact, the HP closure follows from the exact closure procedure for one-dimensional three-moment fluid equations. The derivation of the exact linear closure is one of the results of this work, where I have used the Chapman-Enskog approach [1].

2.1 Hammett-Perkins closure

In the Hammett-Perkins [11] (HP) approach the Landau-fluid (LF) closure operator is the semi-empirical closure. It is obtained by matching the response function in the fluid model with the asymptotic of the exact kinetic expression. It was built in a way to match the exact linear-response function (1.81), close to collisionless, Maxwellian plasma. This section provides the review the three-moment and four-moment fluid models with the closure ansatzes, proposed in HP work.

2.1.1 Three-moment Landau-fluid closure

For a three-moment fluid model, the authors consider the following generalized set of fluid equations for the particle density n , the momentum density mnv , and the pressure p :

$$\frac{\partial n}{\partial t} + \frac{\partial}{\partial z}(vn) = 0, \quad (2.1a)$$

$$\frac{\partial}{\partial t}(mnv) + \frac{\partial}{\partial z}(vmnv) = -\frac{\partial p}{\partial z} + enE - \frac{\partial S}{\partial z}, \quad (2.1b)$$

$$\frac{\partial p}{\partial t} + \frac{\partial}{\partial z}(vp) = -(\Gamma - 1)(p + S)\frac{\partial v}{\partial z} - \frac{\partial q}{\partial z}, \quad (2.1c)$$

where Γ is the ratio of specific heats, and S is dissipative momentum flux, and the heat flux moment is $q = m \int dv f(u - v)^3$. It will be shown further in this Chapter that Eqs. (2.1) are exact moments of Vlasov equation (1.11) in one-dimensional case. They also will correspond to the assumption of $\Gamma = 3$ and $S = 0$ in Eqs. (2.1) made by the authors of this model.

The system of Eqs. (2.1) contain more unknowns than the number of equations and require a closure. The authors came up with two ansatzes: for the heat flux q and dissipative momentum flux S . They were expressed through the lower moments such as the velocity v and the temperature T . The postulated linear closures are written in the form

$$\tilde{q}_k = -n_0\chi_1 \frac{2^{1/2}v_t}{|k|} ik\tilde{T}_k, \quad (2.2)$$

and

$$\tilde{S} = -mn_0\mu_1 \frac{2^{1/2}v_t}{|k|} ik\tilde{v}_k, \quad (2.3)$$

where χ_1, μ_1 are constants. This form is suggested by the dimensional arguments and a further comparison with exact kinetic results. By linearizing the system of Eqs. (2.1) and solving it for density, one finds

$$n = -n_0 \frac{e\phi}{T_0} \mathbf{R}_3, \quad (2.4)$$

where \mathbf{R}_3 is the response function (1.81) for the three-moment fluid model. It is expressed in the form

$$\mathbf{R}_3 = \frac{\chi_1 - i\zeta}{\chi_1 - i\Gamma\zeta - 2i\chi_1\mu_1\zeta - 2\chi_1\zeta^2 - 2\mu_1\zeta^2 + 2i\zeta^3}, \quad (2.5)$$

where $\zeta = \omega/(\sqrt{2}|k|v_T)$ is the normalized frequency. Expansion for \mathbf{R}_3 in the cold plasma limit with $\zeta \gg 1$ is given by:

$$\mathbf{R}_3 \approx -\frac{1}{2\zeta^2} + \frac{1}{2}i\mu_1\frac{1}{\zeta^3} + \left(\frac{1}{2}\mu_1^2 - \frac{3}{4}\right)\frac{1}{\zeta^4}. \quad (2.6)$$

By comparing this expansion to the exact linear response function approximation (1.83) it can be seen that one requires $\mu_1 = 0$ in order to match the exact response function. This explains $S = 0$ in this model. An expansion for R_3 in the case of hot plasma limit with $\zeta \ll 1$:

$$R_3 \approx 1 + 2i\zeta \left(\mu_1 + \frac{1}{\chi_1} \right) - \zeta^2 \left(4\mu_1^2 + 8\frac{1}{\chi_1} + \frac{36}{\chi_1^2} - 2 \right). \quad (2.7)$$

Comparing to the exact plasma response function approximation (1.82) and setting $\mu_1 = 0$, one obtains

$$R_3 \approx 1 + 2i\zeta/\chi_1. \quad (2.8)$$

In order to match the Maxwellian response function $R(\zeta)$ (1.81) for a small argument, the constant can be found as $\chi_1 = 2/\sqrt{\pi}$. Even though χ_1 is chosen this way to fit the low-frequency limit, the closure is for the use in fluid equations, which are automatically valid in the high-frequency limit. The resulting R_3 does a fair job of approximating the Maxwellian R over the full frequency range (Fig. 2.1).

2.1.2 Four-moment Landau-fluid closure

To obtain a more accurate result, a four-moment fluid model was considered by adding an equation for the heat flux q to the system (2.1):

$$\frac{\partial q}{\partial t} + \frac{\partial}{\partial t}(vq) = -3q \frac{\partial u}{\partial z} + 3 \frac{p}{mn} \frac{\partial p}{\partial z} - \frac{\partial r}{\partial z}, \quad (2.9)$$

where

$$r = m \int du f(u-v)^4 = 3p^2/mn + \delta r \quad (2.10)$$

is a higher-order moment. Proposed linear low-frequency closure expression for δr were expressed through the lower order moments, given by

$$\delta \tilde{r}_k \approx -D_1 \frac{\sqrt{2}v_t}{|k|} ik \tilde{q}_k + \beta_1 n_0 2v_t^2 \tilde{T}_k, \quad (2.11)$$

where D_1, β_1 are constants. Following the same procedure and solving linearized four-moment fluid system (2.1, 2.9), a new response function can be obtained:

$$R_4 = \frac{2\beta_1 - 2iD_1\zeta - 2\zeta^2 + 3}{3 + 2\beta_1 - 6iD_1\zeta - (12 + 4\beta_1)\zeta^2 + 4iD_1\zeta^3 + 4\zeta^4}. \quad (2.12)$$

Expanding R_4 in the cold plasma limit $\zeta \gg 1$

$$R_4 \approx -\frac{1}{2\zeta^2} - \left(\frac{1}{2}D_1^2 + \frac{3}{4}\right) \frac{1}{\zeta^4}, \quad (2.13)$$

one can see that it is already satisfied Maxwellian R (1.83) for the second order term. Expanding R_4 for small ζ leads to

$$R_4 \approx 1 + \zeta \frac{4iD_1}{2\beta_1 + 3} + \zeta^2 \frac{8\beta_1^2 + 32\beta_1 - 24D_1^2 + 30}{4\beta_1^2 + 12\beta_1 + 9}. \quad (2.14)$$

To match the Maxwellian R (1.82), a simple system must be solved:

$$\frac{4iD_1}{2\beta_1 + 3} = i\sqrt{\pi}, \quad (2.15)$$

$$\frac{8\beta_1^2 + 32\beta_1 - 24D_1^2 + 30}{4\beta_1^2 + 12\beta_1 + 9} = -2. \quad (2.16)$$

Solving these two equations gives us $D_1 = 2\sqrt{\pi}/(3\pi - 8)$ and $\beta_1 = (32 - 9\pi)/(6\pi - 16)$. Thus, this result is accurate through second order in ζ , while closure for \tilde{q}_k was only first-order accurate. The resulting response function shows much better consistency with the Maxwellian R over the full frequency range (Fig. 2.1).

2.2 Closure model for the heat flux

In this section I derive the linear closure using the Chapman-Enskog approach [1]. Contrary to the Hammet-Perkins methods, the generalized Hammet-Perkins approach result in the exact closure. The fluid equations with the exact closure result in the plasma response which is fully identical to that one obtained from linear kinetic calculations. I also show in this section that the Hammet-Perkins result follows from the exact closure as a leading term of the expansion in the $\omega/(kv_T)$ parameter. The next order terms are also derived in this section.

2.2.1 One-dimensional moment equations

One-dimensional moment equations are considered, which are just a special case of three-dimensional equations (1.23, 1.34, 1.36) when only the longitudinal (along the magnetic field)

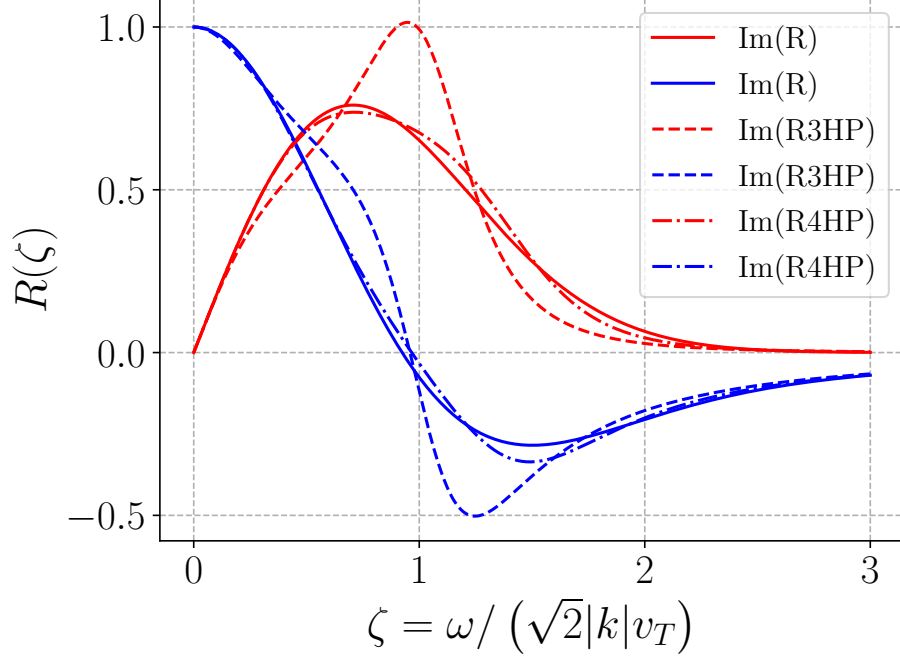


Figure 2.1: The real and imaginary parts of the normalized response function $R(\zeta)$ versus the normalized real frequency ζ .

motion is considered, along the z direction. The resulting moments of the one-dimensional Vlasov equation (1.69) have the form:

$$\frac{\partial}{\partial t} n + \frac{\partial}{\partial z} (nV_{\parallel}) = 0, \quad (2.17)$$

$$\frac{\partial}{\partial t} (nV_{\parallel}) + \frac{\partial}{\partial z} \left(\frac{p_{\parallel}}{m} + nV_{\parallel}^2 \right) + \frac{en}{m} E_{\parallel} = 0, \quad (2.18)$$

$$\frac{\partial}{\partial t} (p_{\parallel} + nV_{\parallel}^2) + \frac{\partial}{\partial z} (2q_{\parallel} + 3V_{\parallel}p + nV_{\parallel}^3) - \frac{2en}{m} E_{\parallel} V_{\parallel} = 0, \quad (2.19)$$

$$\frac{\partial}{\partial t} (2q_{\parallel} + 3V_{\parallel}p + nV_{\parallel}^3) + \frac{\partial}{\partial z} (r_{\parallel} + 4q_{\parallel}V_{\parallel} + 6\frac{p_{\parallel}}{m}V_{\parallel}^2 + nV_{\parallel}^4) + \frac{4e}{m} E_{\parallel} \left(\frac{p_{\parallel}}{m} + nV_{\parallel}^2 \right) = 0, \quad (2.20)$$

with the following definition of macroscopic variables. The density is

$$n = \int f(v_{\parallel}) dv_{\parallel}, \quad (2.21)$$

the fluid velocity V_{\parallel} ,

$$nV_{\parallel} = \int f(v_{\parallel}) v_{\parallel} dv_{\parallel}, \quad (2.22)$$

the pressure moment p_{\parallel}

$$p_{\parallel} = m \int f(v_{\parallel}) v_{\parallel}'^2 dv_{\parallel}', \quad (2.23)$$

where v_{\parallel}' is the random particle velocity, such that $v_{\parallel} = v_{\parallel}' + V_{\parallel}$ and it obeys $\int f(v_{\parallel}) v_{\parallel}' dv_{\parallel}' = 0$ condition. The heat flux is defined as

$$q_{\parallel} = \frac{m}{2} \int f(v_{\parallel}) v_{\parallel}'^3 dv_{\parallel}', \quad (2.24)$$

and the next (fourth) moment macroscopic variable r_{\parallel} is

$$r_{\parallel} = m \int f(v_{\parallel}) v_{\parallel}'^4 dv_{\parallel}'. \quad (2.25)$$

After some rearrangements, let us can write the first three moments, Eqs. (2.17-2.19) as

$$\frac{\partial n}{\partial t} + \frac{\partial}{\partial z}(vn) = 0, \quad (2.26a)$$

$$mn \left(\frac{\partial}{\partial t} + v \frac{\partial}{\partial z} \right) v = -\frac{\partial p}{\partial z} + enE, \quad (2.26b)$$

$$\frac{\partial p}{\partial t} + \frac{\partial}{\partial z}(vp) = -2p \frac{\partial v}{\partial z} - 2 \frac{\partial q}{\partial z}, \quad (2.26c)$$

where the parallel indices are omitted. This system is used in further kinetic closure derivation. In comparison to the Hammett-Perkins three-moment model (2.1), the system (2.26) does not contain the friction variable S . HP artificially introduced this dissipative momentum flux in order to compare with previously suggested Landau damping models [9].

2.2.2 Chapman-Enskog method for heat flux closure derivation

System (2.26) contains the unknown heat flux q , which needs to be evaluated in order to close the system. The goal of this derivation is to find the heat flux in a form, that allows incorporating some kinetic effects into a fluid system of plasma equations. For this purpose plasma fluid equations and kinetic equation are combined. The approach is based on the Chapman-Enskog [1] ansatz, which presents the distribution function in the following form:

$$f = f_M + \tilde{F}, \quad (2.27)$$

where f_M is the dynamical Maxwellian and \tilde{F} is the small deviation. The dynamical Maxwellian is given by

$$f_M = \frac{n(x, t)}{\pi^{1/2} [2T(x, t)/m]^{1/2}} \exp\left(-\frac{m[v - V(x, t)]^2}{2T(x, t)}\right), \quad (2.28)$$

where the macroscopic variables of density $n(x, t)$, temperature $T(x, t)$, and flow velocity $V(x, t)$ are time and spatially dependent. This allows the distribution function to evolve in time and space accordingly to the first three fluid moments (2.26). A variable v in (2.28) is the particle velocity, therefore $v' = v - V$ is the random part of velocity. Also, the ansatz (2.27) implies that the deviation \tilde{F} does not contribute to the lower moments $n(x, t)$, $T(x, t)$, and $V(x, t)$. This condition is expressed by the following constraints:

$$\int \tilde{F} \{1, v', mv'^2/2\} d^3v' = 0. \quad (2.29)$$

By substituting Eq. (2.27) into one-dimensional Vlasov equation (1.69), I have obtained:

$$\begin{aligned} D\tilde{F} + \left(\frac{\partial n}{\partial t} + v\frac{\partial n}{\partial x}\right) \frac{F_m}{n} + \left(\frac{\partial T}{\partial t} + v\frac{\partial T}{\partial x}\right) \left(-\frac{1}{2} + \frac{v'^2}{v_T^2}\right) \frac{F_m}{T} \\ + \left(\frac{\partial V}{\partial t} + v\frac{\partial V}{\partial x}\right) \cdot \frac{2v'}{v_T^2} F_m + \frac{e}{m} E \frac{\partial F_m}{\partial v} = 0, \end{aligned} \quad (2.30)$$

where

$$D \equiv \frac{\partial}{\partial t} + v\frac{\partial}{\partial x} + \frac{e}{m} E \frac{\partial}{\partial v}. \quad (2.31)$$

The Eq. (2.30) explicitly contains the substantial derivatives of the macroscopic fluid variables n, V, T , which are substituted from the system (2.26) to obtain

$$D\tilde{F} = -v' \frac{\partial T}{\partial x} \left(\frac{3}{2} - \frac{v'^2}{v_T^2}\right) \frac{F_m}{T} + \frac{\partial q}{\partial x} \left(\frac{2v'^2}{v_T^2} - 1\right) \frac{F_m}{p}. \quad (2.32)$$

By linearizing this expression and taking the Fourier transform, I have obtained

$$\tilde{F} = -\frac{\tilde{T}}{T} \frac{kv'F_0}{\omega - kv'} \left(\frac{3}{2} - \frac{v'^2}{v_T^2}\right) + \frac{\tilde{q}}{pv_T} \frac{kv_T F_0}{\omega - kv'} \left(1 - \frac{2v'^2}{v_T^2}\right), \quad (2.33)$$

that can be written in a compact form:

$$\tilde{F} = -\frac{\tilde{T}}{T} a_T + \frac{\tilde{q}}{pv_T} a_q, \quad (2.34)$$

with coefficients

$$a_T = \frac{kv'F_0}{\omega - kv'} \left(\frac{3}{2} - \frac{v'^2}{v_T^2}\right), \quad (2.35)$$

$$a_q = \frac{kv_T F_0}{\omega - kv'} \left(1 - \frac{2v'^2}{v_T^2}\right). \quad (2.36)$$

Integrating Eq. (2.34) over dv' and using condition (2.29), I have obtained the closure expression:

$$\frac{\tilde{q}_k}{pv_T} = Q_t \frac{\tilde{T}_k}{T}, \quad (2.37)$$

where $Q_T = \frac{\overline{a_T}}{\overline{a_q}}$ and

$$\overline{a_T} = \int_{-\infty}^{\infty} \frac{kv'F_m}{\omega - kv'} \left(\frac{3}{2} - \frac{v'^2}{v_T^2} \right) dv', \quad (2.38)$$

$$\overline{a_q} = \int_{-\infty}^{\infty} \frac{kv_T F_m}{\omega - kv'} \left(1 - \frac{2v'^2}{v_T^2} \right) dv', \quad (2.39)$$

and finally, Q_T is found as (integrals used are listed in Appendix C)

$$Q_T = \frac{1 + \frac{3}{2}Z\zeta - \zeta^2 - Z\zeta^3}{Z - 2\zeta - 2Z\zeta^2}. \quad (2.40)$$

To show that the fluid equations (2.26) with closure (2.40) are fully equivalent to the linear kinetic model, I have followed the Hammett-Perkins procedure and found the response function:

$$R(\zeta) = 1 + \zeta Z(\zeta), \quad (2.41)$$

which is the exact response function that was defined in Chapter 1 for electrostatic waves in kinetic theory. The adiabatic limit $\zeta \ll 1$ for Q_T is found approximately to be

$$Q_T \approx -\frac{i}{\sqrt{\pi}} + \zeta \left(\frac{3}{2} - \frac{4}{\pi} \right). \quad (2.42)$$

Substituting only zeroth order term from Eq. (2.42) into Eq. (2.37), the approximate expression for the heat flux closure is:

$$\tilde{q}_k = -\frac{n_0 v_T}{\sqrt{\pi}} \frac{ik\tilde{T}_k}{|k|}, \quad (2.43)$$

which is similar to the three-moment fluid closure (2.2) in the HP model (with corrections should be made on the heat flux q and the thermal velocity v_T definitions). One can evaluate the inverse Fourier transform of the heat flux closure (2.43), to find a real space representation

$$q(z) = -\frac{n_0 v_T}{\sqrt{\pi}} \int_0^{\infty} \frac{T(x+x') - T(x-x')}{x'} dx', \quad (2.44)$$

where the convolution theorem has been used. It shows an intrinsic nonlocality in real space of the obtained closure, i.e. evaluation of the heat flux requires information about energy field in all space. Dealing with nonlocal operators generally requires special numerical treatment and it is introduced in Chapter 3.

If one desire a higher linear accuracy, the next term can be included in our closure (2.37) from Eq. (2.42). In fact, this results in a much better approximation of the response function. Fig. 2.2 shows, that it is comparable to the HP four-moment fluid model with kinetic closure (2.11). However, the transcendental dependence on frequency ω from the second term in (2.42) would need to be addressed. For the general (non-linear) purpose simulations, some kind of instantaneous estimate [39] of ω could be used.

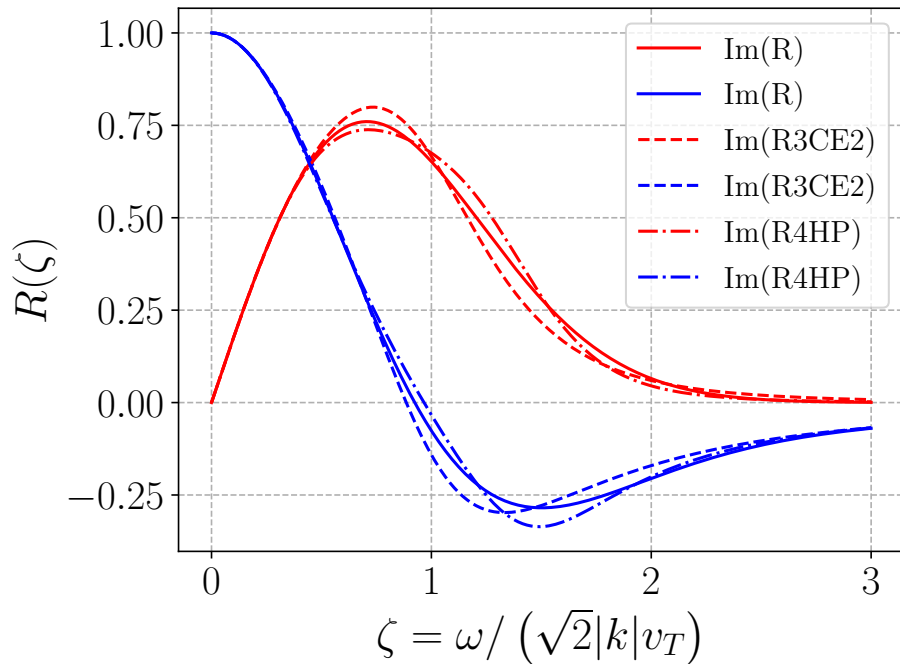


Figure 2.2: Exact kinetic response function presented here with solid lines, HP four-moment LF with dashed lines and our Chapman-Enskog closure (dotted lines) in the first-order approximation, Eq. (2.42).

2.3 Ion sound dispersion relation from the fluid model with the closure

In this section I use the fluid model with closure to derive the self-consistent dispersion relation for the ion sound waves. The goal is to investigate the validity of the kinetic closure (2.37) in the complex frequency plane. The fluid equations for the ion component are

$$\frac{\partial n_i}{\partial t} + \frac{\partial}{\partial z}(v_i n_i) = 0, \quad (2.45a)$$

$$m_i n_i \left(\frac{\partial}{\partial t} + v_i \frac{\partial}{\partial z} \right) v_i = -\frac{\partial p_i}{\partial z} + e n_i E, \quad (2.45b)$$

$$\frac{\partial p_i}{\partial t} + \frac{\partial}{\partial z}(v_i p_i) = -2p_i \frac{\partial v_i}{\partial z} - 2 \frac{\partial q}{\partial z}, \quad (2.45c)$$

where the closure is given with

$$q = -\frac{n_0 v_{T_i}}{\sqrt{\pi}} \frac{ikT_i}{|k|}. \quad (2.46)$$

The Boltzmann relation is used for the electron component. The full system is linearized for small amplitude perturbations:

$$n(x, t) = n_{0i} + \tilde{n}_i(x, t), \quad v_i(x, t) = \tilde{v}_i(x, t), \quad T_i(x, t) = T_{0i} + \tilde{T}_i(x, t). \quad (2.47)$$

Let us seek the solution in the form $\tilde{X} \sim e^{-i(\omega t - kx)}$. Then the linear equations in Fourier space take the form (the tilde signs are omitted here)

$$-i\omega n_i + ikn_{0i}v_i = 0, \quad (2.48a)$$

$$-i\omega m_i v_i + ikT_i + ikT_{0i} \frac{n_i}{n_{0i}} + ike\phi = 0, \quad (2.48b)$$

$$-i\omega T_i + 2ikT_{0i}v_i + \alpha\sqrt{\tau}kc_s T_i = 0, \quad (2.48c)$$

where $\tau = T_{0i}/T_{0e}$, $\alpha = \sqrt{8/\pi}$, $q = -i\sqrt{\tau} \alpha/2 n_0 c_s T_i$. The dispersion relation in the quasineutral case $n_i \approx n_e$ can be found in the form:

$$1 - \frac{k^2 c_s^2}{\omega^2} (1 + \tau) - \tau \frac{2k^2 c_s^2}{\omega^2 + \tau \alpha^2 k^2 c_s^2} + i\tau^{3/2} \frac{\alpha^3 k^3 c_s^3}{\omega (\omega^2 + \tau \alpha^2 k^2 c_s^2)} = 0. \quad (2.49)$$

Analytical solution of this equation can be obtained by the method of perturbation using ion temperature as a small parameter. Thus for ($\tau \ll 1$) one can find

$$\omega = \omega_0 + \frac{3}{2}\tau\omega_0 - i\tau^{3/2}\omega_0\alpha, \quad (2.50)$$

where

$$\omega_0^2 = k^2 c_s^2. \quad (2.51)$$

Therefore, the approximate expression for the damping rate is

$$\gamma = \alpha \tau^{3/2} k c_s. \quad (2.52)$$

In order to compare this linear fluid model with the kinetic result, I have also solved the dispersion equation (2.49) numerically exactly. This solution is shown in Fig. 2.3. The approximate solution (2.52) is valid only for small values of τ , as it is expected.

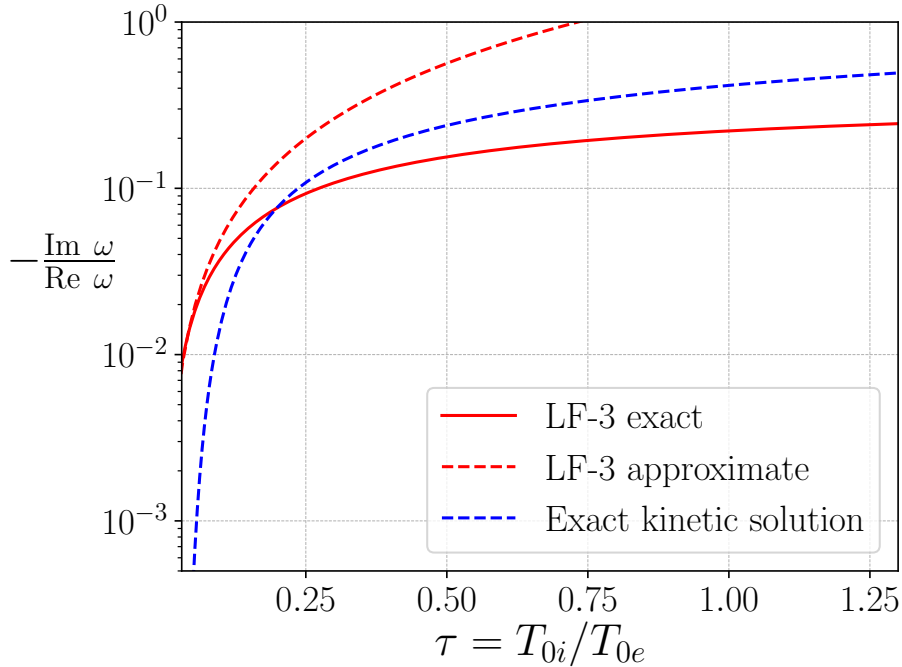


Figure 2.3: Landau damping for three-moment fluid model with kinetic closure (2.46). The exact solution of the dispersion equation (2.49) (red) and the approximate solution (2.52) (red dashed) in comparison with the exact kinetic solution of Eq. (1.89) (blue dashed).

CHAPTER 3

NUMERICAL IMPLEMENTATION OF COLLISIONLESS CLOSURES

In the previous Chapter, we have discussed collisionless closure for fluid plasma equations. Also, the exact linear kinetic closure was derived. In this Chapter, the numerical methods for solving these closure operators are introduced, as well as the verification procedure. Collisionless kinetic closures naturally arise in a Fourier space, however, they are intrinsically nonlocal due to the presence of the nonlocal operator $\text{sgn}(k) = k/|k|$ (2.43). Often simulations are performed in real space and (Fourier) transform to real space results in greater computational cost. One of the methods that was developed recently, the fast non-Fourier method [12], allows efficiently to perform such calculations with kinetic closure operators in real space. As the part of this thesis, I have implemented numerical simulation, involving the fast non-Fourier method. It was done in the BOUT++ framework [13], that has been used for the calculations of the fluid plasma equations with the fast non-Fourier method. For verification purposes, I have used the simulations with three- and four-moment one-dimensional linear equations with the kinetic closures. From these simulations, the plasma response function was compared with the exact kinetic result. It showed excellent agreement between fast non-Fourier method and Fourier space calculations. Further, ion Landau damping problem has been studied using the simulation for the three-moment fluid model. Let us start with the description of the fast non-Fourier method.

3.1 Fast non-Fourier method for the computation of closure operators

The closure operator (2.43) has a relatively simple form in Fourier space. However, in many cases, the simulations are performed in the real space because of complex geometry, spatial nonuniformity, and nonlinear effects. For these cases, operators become nonlocal and Fourier representation becomes less useful. Conversions between the real and Fourier space can become more time consuming, particularly when one wants to perform such transformation on the nonlocal operator $\text{sgn}(k)$. Such conversions to real space may require an additional computational cost. Therefore, an effective non-Fourier method is needed.

The fast non-Fourier method [12, 40, 41] represents a closure operator $\text{sgn}(k)$ as a system of equations in the real space. It is based on the approximation of the term $1/|k|$ with a sum of Lorentzian functions in Fourier space, which correspond to the solution of modified Helmholtz equation in real number space. The inhomogeneous modified Helmholtz equation is

$$\left(1 - \frac{\partial^2}{\partial z^2}\right) \psi(z) = S(z), \quad (3.1)$$

where z is a single real spatial variable, $S(z)$ is the source function. It was shown [12] that multiplication of the field S by $1/(1+k^2)$ is equivalent of applying the inverse of a modified Helmholtz operator.

The $1/|k|$ part of the $\text{sgn}(k)$ can be approximated with the finite sum of Lorentzians $\psi_N(k)$ [12]:

$$\frac{1}{|k|} \approx \psi_N(k) = \beta \sum_{n=0}^{N-1} \frac{\alpha^n}{k^2 + \alpha^{2n}}, \quad (3.2)$$

where N is a positive integer. Convenient choice of constants α, β , N allows a good fit in Fourier space over a wide range of the wavenumber k . By using proposed [12] parameters $\alpha = 5, \beta = 1.04$ and $N = 7$ gives a 2% relative error over approximately 10^3 spectral range. It is illustrated in Fig. 3.1 with a plot of $|k|\psi_7(k)$, where

$$\psi_7(k) = 1.04 \sum_{n=0}^6 \frac{5^n}{k^2 + 5^{2n}}. \quad (3.3)$$

Such an approximation is sufficient for many simulations. However, if one needs a different range of wavenumber with a good fit, it can be “shifted”. With a multiplier k_0 for α in Eq. (3.3) it can be shifted to lower ($k_0 < 1$) or higher ($k_0 > 1$) wavenumber region. It is illustrated in Fig. 3.2.

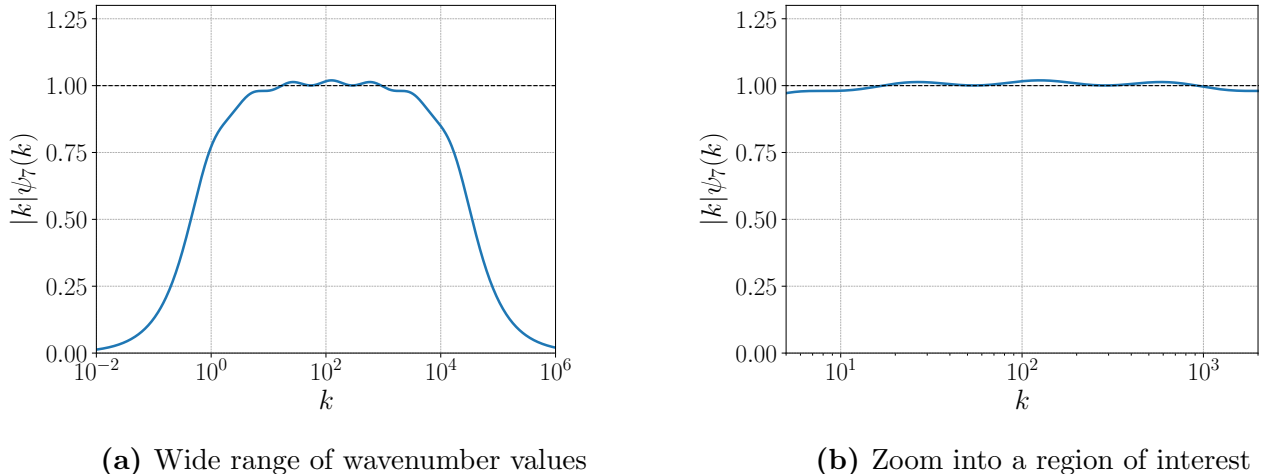


Figure 3.1: Plot of $|k|\psi_7(k)$, where $\psi_7(k)$ (3.3) is the approximation for $1/|k|$. Therefore, region of good fit is around one; (a) shows a wide range of wavenumber values, including regions, where approximation becomes not valid; (b) represents the same plot within range of good fit.

3.2 BOUT++: High Performance fluid simulations framework

As mentioned previously, to perform our simulations, the BOUT++ framework was used. This code created at the Los Alamos National Laboratory and widely used worldwide for simulations of tokamak plasmas. BOUT++ is a modular platform for 3D simulations of an arbitrary number of fluid equations in curvilinear coordinates using finite-difference methods [13,42]. It was developed based on the original BOUndary Turbulence (BOUT) 3D 2-fluid code [43, 44]. BOUT++ uses the coordinate system metric tensor $g^{ij} = g^{ij}(x, y)$ (constant in one dimension), therefore it is restricted to the coordinate system with axi- or translationally symmetric geometry. The two-dimensional metric tensors allow the code to be used to simulate plasmas in many geometries like slab, sheared slab, cylindrical coordinates, etc.

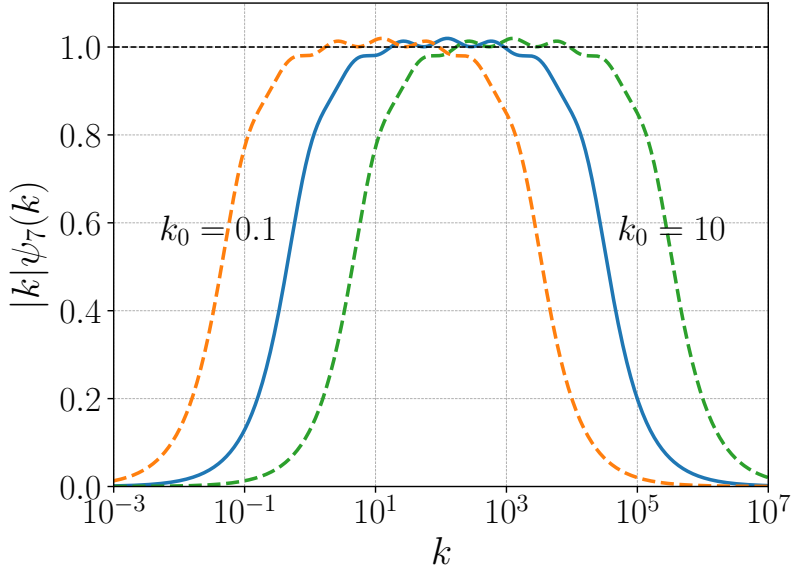


Figure 3.2: Plot of $|k|\psi_7(k)$, where $\psi_7(k)$ (3.3) is the approximation for $1/|k|$. It can be “shifted” into lower and higher wavenumber region using a multiplier k_0 for α in Eq. (3.3); solid blue line corresponds to $k_0 = 1$.

BOUT++ has the object-oriented framework in C++ and able to perform parallel computations with a good efficiency up to thousands of processors. BOUT++ is a free open-source project that is being constantly developed [45] by many users.

The structure of BOUT++ allows separating general blocks of curvilinear geometry, differential geometry, parallel communication, numerical solvers, and others, from the problem specific physical equations. The BOUT++ philosophy was to allow the user to concentrate on physics as much as possible, selecting the most efficient numerical approaches while reusing some highly efficient numerical blocks, e.g. massively parallel communication between the cores. However, choosing particular schemes, geometry, boundary conditions, etc. is wholly problem-specific, and requires a good knowledge of computational fluid dynamics [46] and programming skills.

The core of BOUT++ is written in C/C++, it is organized into classes and functions which operate on them. Fig. 3.3 represents the main parts of the code and operations flow during initialization and run. The initialization (shown in red) starts with `physics_init` function reading a grid file (information on the mesh size, geometry configuration etc.). This

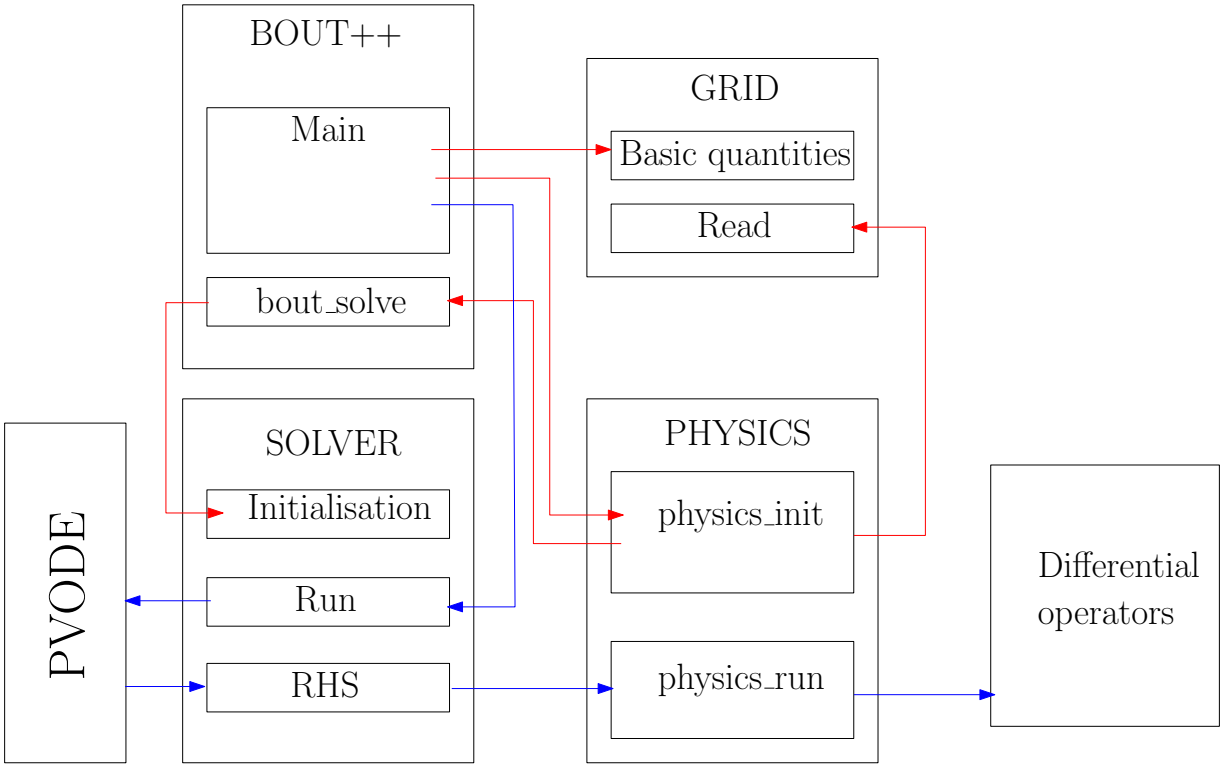


Figure 3.3: Overview of the BOUT++ control flow during initialization (red), and during running a simulation (blue) [45].

step can be replaced by the reading from the user specified input file. Then `physics_init` continues, it reads if necessary additional parameters and variables from the grid or/and input file, and specify variables to be evolved. It calls `bout_solve` function to pass these variables to the solver. Running operation (shown in blue) starts when the `Main` function calls the solver. While it is initialized, it calls a corresponding solver, which is PVODE by default (can be replaced). To advance equations, PVODE makes calls to `RHS` function, which, in turn, calls `physics_run` function, where user-specified equations are written. `Physics_run` mostly does calculations of the differential operators, and inversion operations (e.g., Poisson equation) if they are present in a given model. This is a rough general scheme which misses many other operations, such as memory handling, parallelization etc.

The space coordinates x, y, z in BOUT++ are not all equivalent. As it was mentioned, metric tensor implies some restrictions on the geometry configuration: z -direction is always periodic, x and y can be either periodic or bounded. By convention, y -coordinate in BOUT++ is parallel to magnetic field lines direction. Thus, the (x, z) plane is the perpen-

dicular plane to the magnetic field lines. BOUT++ supports either scalar or vector fields and includes a wide range of differential operators that can be applied to all variables. Gradient operators in perpendicular and in parallel directions to the magnetic field are implemented in order to take advantage of the length-scale separation.

Time integration in BOUT++ is implemented with the various solvers, such as PVODE, CVODE, Euler, Runge-Kutta, PETSc, and other. The CVODE [47] is a commonly used solver, it solves stiff and non-stiff systems of ordinary differential equations. It does not require the information about a structure of the equations, solving initial value problems (IVPs) of the form:

$$\frac{d\mathbf{f}}{dt} = g(\mathbf{f}, t), \quad (3.4)$$

$$\mathbf{f}(t_0) = \mathbf{f}_0, \quad (3.5)$$

where $g(\mathbf{f}, t)$ is a general nonlinear function, which does not contain time derivatives of \mathbf{f} . The methods are implemented in the CVODE adjust the internal time-step and order to satisfy requested tolerances. The BOUT++ code calculates the nonlinear function $g(\mathbf{f}, t)$ with finite-difference methods. These include central derivatives (first and second derivatives), advection schemes in each dimension separately, and flux conserving methods of various order.

Additionally, BOUT++ includes methods for Laplacian inversion (e.g., for solving Poisson equation), both in parallel (y -direction) and perpendicular ((x, z) -plane) directions. In parallel direction, it allows to inverse an equation of the following form:

$$(A + B\nabla_{\parallel}^2) \phi = \rho, \quad (3.6)$$

where ϕ is an unknown scalar field and ρ is a (known) scalar field input. It is being solved accordingly to the boundary conditions. For the periodic domain the cyclic reduction is implemented.

BOUT++ uses two input files: an options text file and a binary grid file. Option file is used for setting numerical schemes, boundary conditions, simulation time. Binary grid file is used for the geometry configuration, mesh space, and initializing of evolving variables. However, in the most recent revisions of the code geometry parameters can be also specified in the options text file. This includes metric tensor components and a wide range of the initial conditions for each evolving variable. This allows skipping grid file for many problems.

My one-dimensional simulations of three- and four- moment plasma fluid model required to advance three and four linear equations in time, respectively; along with solving of the Helmholtz equation for the closure term at each time step. Parallel y -direction in BOUT++ was the best choice here, it is periodic by default and allows calculating the inverse of Helmholtz equation (3.1), with $A = 1$ and $B = -1$ in Eq (3.6). The CVODE time solver with the parameters `atol` = 10^{-10} , `rtol` = 10^{-5} was used for all simulations in this thesis. Such tolerances are usually sufficient for normalized equations. While our equations have no upwind terms of the form $v \partial v / \partial x$, the central finite-difference scheme of the second order was set for all spatial derivative calculations.

3.3 Evaluation of plasma response function

To check the accuracy and verify the fast non-Fourier method implementation, let us evaluate the response function for a given Landau-fluid model. The plasma response function is defined as the response of the perturbed density to the potential perturbation (1.85). For simplicity it is presented in the dimensionless form: (see the normalization scheme later in this section)

$$\tilde{n}(k, \omega) = -\tilde{\phi}(k, \omega)R(k, \omega). \quad (3.7)$$

To evaluate R for a system of linear plasma fluid equations, let us introduce the external potential of the form $\phi_{ext} \sim \sin(kz - \omega t)$. This can be used as the driving force for a system of linear plasma fluid equations, where one can expect (the system is linear) that the perturbed density solution will settle on $\tilde{n}(k, z) = A(k, z) \sin(kz - \omega t + \delta)$. The amplitude A and phase shift δ depends on driven frequency ω and wavenumber k . Then the plasma response function R can be evaluated from (3.7) as

$$\text{Re}(R) = A \cos(\delta), \quad (3.8a)$$

$$\text{Im}(R) = -A \sin(\delta). \quad (3.8b)$$

By varying the frequency ω with the fixed wavenumber k in driving force, the plasma response function R can be evaluated over the range of frequencies.

3.3.1 Three-moment Landau-fluid model

The equations to be solved will be presented in dimensionless form, to reduce roundoff errors and the number of parameters in the equations. A normalization scheme is introduced as

$$n' = \frac{n}{n_0}, \quad T' = \frac{T}{T_{0i}}, \quad \phi' = \frac{e\phi}{T_{0e}}, \quad v' = \frac{v}{c_s}, \quad q' = \frac{q}{c_s T_{0i} n_0}, \quad t' = w_{pi} t, \quad z' = \frac{z}{\lambda_D}. \quad (3.9)$$

Using the linearization scheme (2.47), our normalized system for the three-moment fluid model, obtained from Eqs. (2.26) is (prime signs are omitted for normalized variables and tilde signs are skipped for linearized variables):

$$\frac{\partial n}{\partial t} + \frac{\partial v}{\partial z} = 0, \quad (3.10a)$$

$$\frac{\partial v}{\partial t} + \frac{\partial n}{\partial z} + \frac{\partial T}{\partial z} + \frac{\partial \phi_{ext}}{\partial z} = 0, \quad (3.10b)$$

$$\frac{\partial T}{\partial t} + 2\frac{\partial v}{\partial z} + 2\frac{\partial q}{\partial z} = 0, \quad (3.10c)$$

where ϕ_{ext} represents the driving force $\phi_{ext} = \sin(kz - \omega t)$. The heat flux q for this model is taken in the zero-order approximation (2.43) in order to apply the fast non-Fourier method. Rewritten in the dimensionless form, the heat flux closure is:

$$q_k = -\sqrt{\frac{2}{\pi}} \frac{1}{|k|} ikT_k. \quad (3.11)$$

Following the fast non-Fourier method, the $1/|k|$ part is approximated with the partial sum $\psi_N(k)$, Eq. (3.2). This implies that the heat flux is also represented by the partial sum:

$$q_k = \sum_{n=0}^{N-1} q_k^n, \quad (3.12)$$

where each term q_k^n has the form

$$q_k^n = -\sqrt{\frac{2}{\pi}} \beta \frac{\alpha^n}{k^2 + \alpha^{2n}} ikT, \quad (3.13)$$

and after simple rearrangement, one obtains a familiar structure of the modified Helmholtz equation (3.1):

$$(k^2 + \alpha^{2n}) q_k^n = -\chi_1 2^{1/2} \beta \alpha^n ikT. \quad (3.14)$$

It is possible to evaluate operators of the form $k^n \leftrightarrow (-i\partial/\partial z)^n$ to transform the Eq. (3.14) to real space:

$$\left(\alpha^{2n} - \frac{\partial^2}{\partial z^2}\right) q^n(z) = -\chi_1 2^{1/2} \beta \alpha^n \frac{\partial T(z)}{\partial z}. \quad (3.15)$$

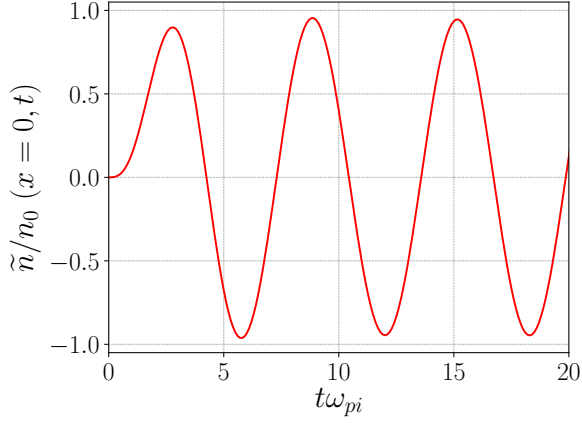
Finally, the numerical solution for the total heat flux q can be found by the summation over all the partial solutions of Eq. (3.15):

$$q(z) = \sum_{n=0}^{N-1} q^n(z), \quad (3.16)$$

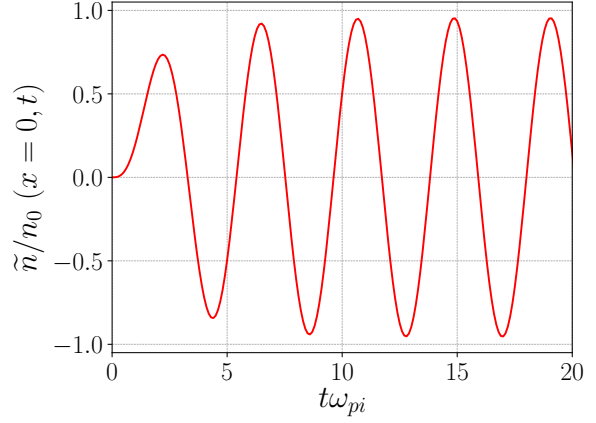
where Eq. (3.15) is solved for each partial heat flux term $q^n(z)$ at every time step.

Thus, the total system consists of equations are Eqs. (3.10) along with N Eqs. (3.15) for the closure approximation, where N is the number of series elements in the Eq. (3.16).

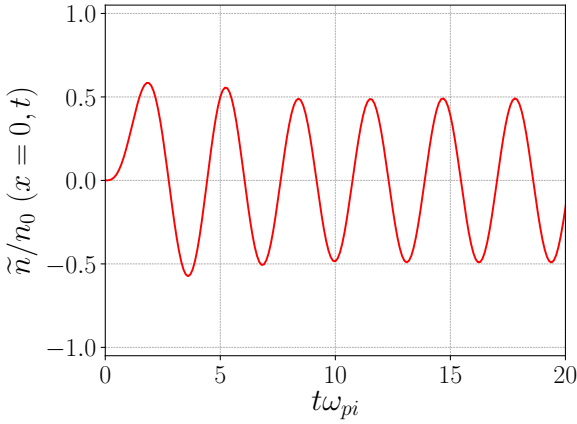
As it was expected, an externally driven potential made the plasma density $n(k, w)$ to settle on a sinusoidal solution, as shown in Fig. 3.4. An example of such density response is shown in Fig. 3.5, where the system was driven with frequency $\omega = 2\omega_{pi}$. The phase shift between the plasma density response and the external potential δ and the amplitude of the density response A , substituted to Eqs. (3.8), are used to evaluate the plasma response function R at the point $\zeta = 2\omega_{pi}/v_T$ ($k = 1$). In this way, it is possible to plot the plasma response function over the frequencies for the three-moment model with Hammett-Perkins closure ansatz, Fig. 3.6. It shows good accuracy and excellent agreement with the analytical plasma response function (Fourier space calculations) [48].



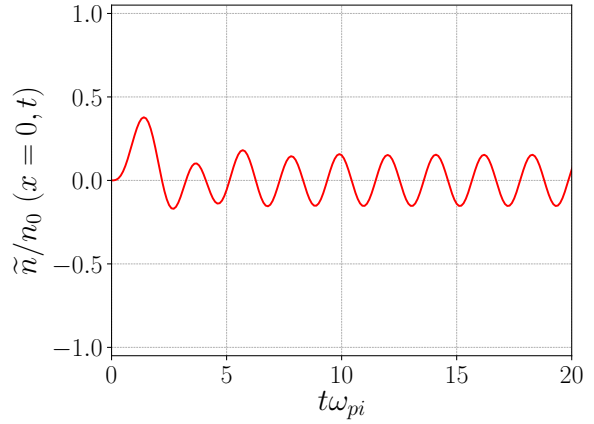
(a) $\phi_{ext} \sim \sin(0.5\omega_{pi}t)$



(b) $\phi_{ext} \sim \sin(\omega_{pi}t)$



(c) $\phi_{ext} \sim \sin(2\omega_{pi}t)$



(d) $\phi_{ext} \sim \sin(3\omega_{pi}t)$

Figure 3.4: Plasma density response for externally driven potential, for several driven frequencies. The different amplitude response (smaller for higher frequency) can be noted. The solution settles to the constant sine form after ~ 10 ion plasma periods, after what the evaluation of the plasma response function (3.8) can be performed.

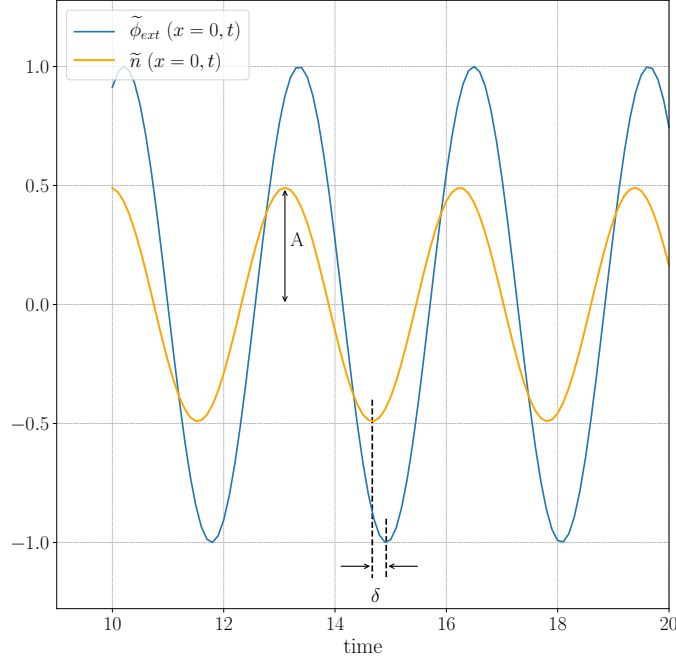


Figure 3.5: The plasma density response \tilde{n} for the externally driven potential $\tilde{\phi}_{ext} \sim \sin(2\omega_{pi}t)$. The phase shift δ between the driven wave and the response, along with the amplitude A of the density response are used to evaluate the plasma response function (3.8).

3.3.2 Improvement to the three-moment kinetic closure

As shown in Chapter 2, our kinetic closure (2.42) for the heat flux with the second term (in $\zeta \ll 1$ limit) provides a better approximation for the response function. It is worth to try to include it to the simulation. Let us write the expression for q , using Eq. (2.42): (in a dimensionless form)

$$q_k = -\sqrt{\frac{2}{\pi}} \frac{1}{|k|} ikT_k + \frac{\omega}{|k|} \left(\frac{3}{2} - \frac{4}{\pi} \right) T_k, \quad (3.17)$$

where $\omega/|k|$ should be estimated somehow. In this particular simulation, the the system is driven with the external force with the frequency ω and fixed wavenumber k . Thus, I have tried to substitute these values of k and ω into the Eq. (3.17). Such an assumption results in a good agreement between BOUT++ simulations and the Fourier result for plasma response

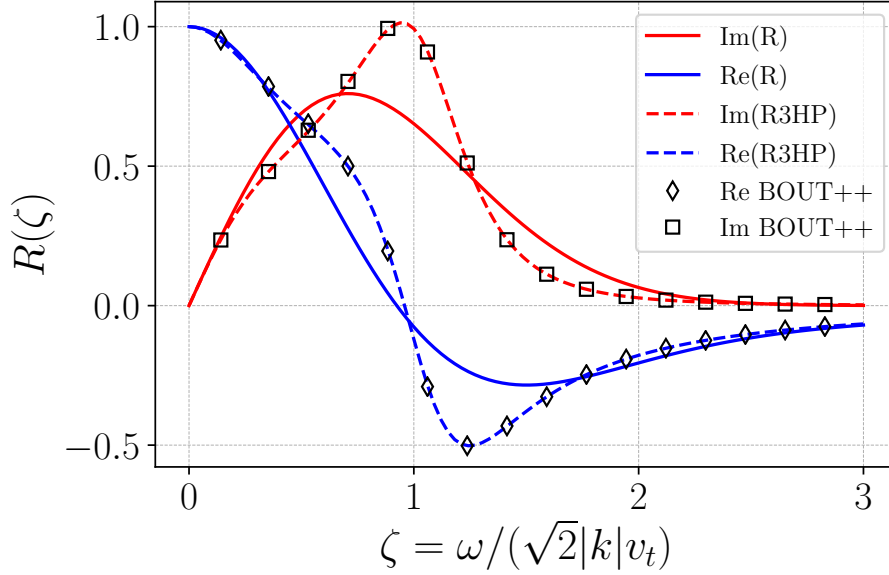


Figure 3.6: The real and imaginary parts of the normalized response function for the three-moment model (with BOUT++ non-Fourier calculations) with HP-like closure (3.11) compared to the exact response function.

function (Fig. 3.7).

3.3.3 Four-moment Landau-fluid model

It is of interest to apply the same procedure to the four-moment system of fluid plasma equations, where the heat flux q evolves accordingly to the next moment of the Vlasov equation. This moment for the heat flux q is given in (2.9), with the closure (2.11), proposed in the HP work. The system of linear equations (3.10) thus must be supplemented with the linear heat flux moment:

$$\frac{\partial q}{\partial t} + 3\frac{\partial v}{\partial z} + \frac{\partial(\delta r)}{\partial z} = 0, \quad (3.18)$$

where r variable is normalized as $r' = r/(n_0 c_s^2 T_0)$. Closure term δr (2.11) in the dimensionless form is

$$\delta \tilde{r}_k = -D_1 \frac{\sqrt{2}}{|k|} ik \tilde{q}_k + 2\beta_1 \tilde{T}_k, \quad (3.19)$$

where constants $D_1 = 2\sqrt{\pi}/(3\pi - 8)$ and $\beta_1 = (32 - 9\pi)/(6\pi - 16)$. Note, that the second term in closure term (3.19) is local and can be simply converted to real space. Therefore, the

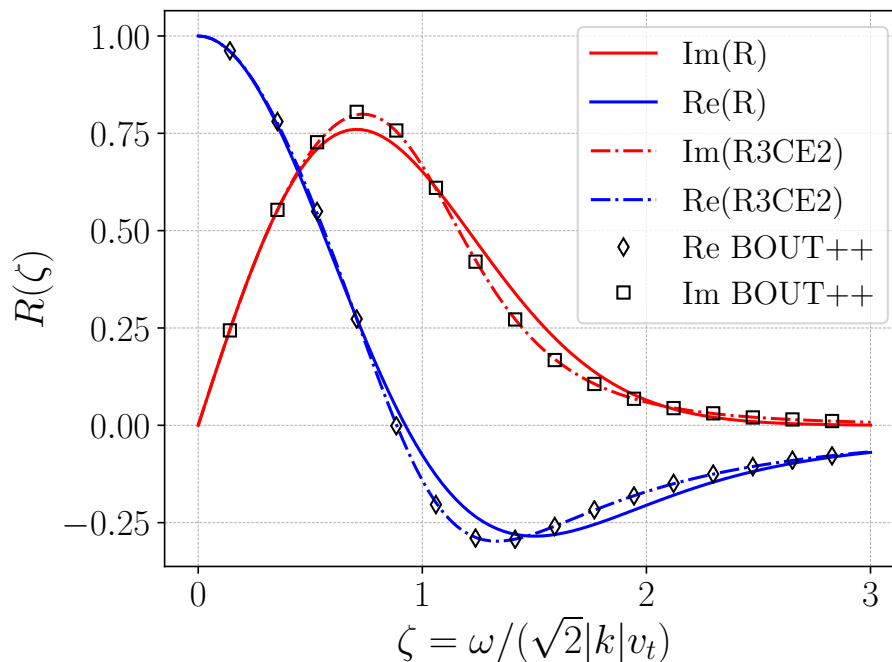


Figure 3.7: The real and imaginary parts of the normalized response function for the three-moment model (with BOUT++ non-Fourier calculations) with improved closure (3.17) compared to the exact response function.

procedure of the fast non-Fourier method is applied to the first term only. The same $\psi_7(k)$ (3.3) was used to approximate $1/|k|$ term in Eq. (3.19), and externally driven simulation was performed to evaluate the plasma response function. The resulting response function is given in Fig. 3.8, it also shows excellent agreement with the Fourier calculations.

3.4 Landau damping with kinetic closure

In the previous section the closures were verified by evaluating a response of the plasma component to the applied electric field. Another verification of kinetic closures can be performed in the self-consistent simulation of the Landau damping. Let us use the three-moment fluid model 3.20a) with the kinetic closure for the heat flux (3.11). A self-consistent model should contain electron dynamics as well. The Boltzmann relation for electrons (1.64) has been used together with quasineutrality approximation. Using the same normalization

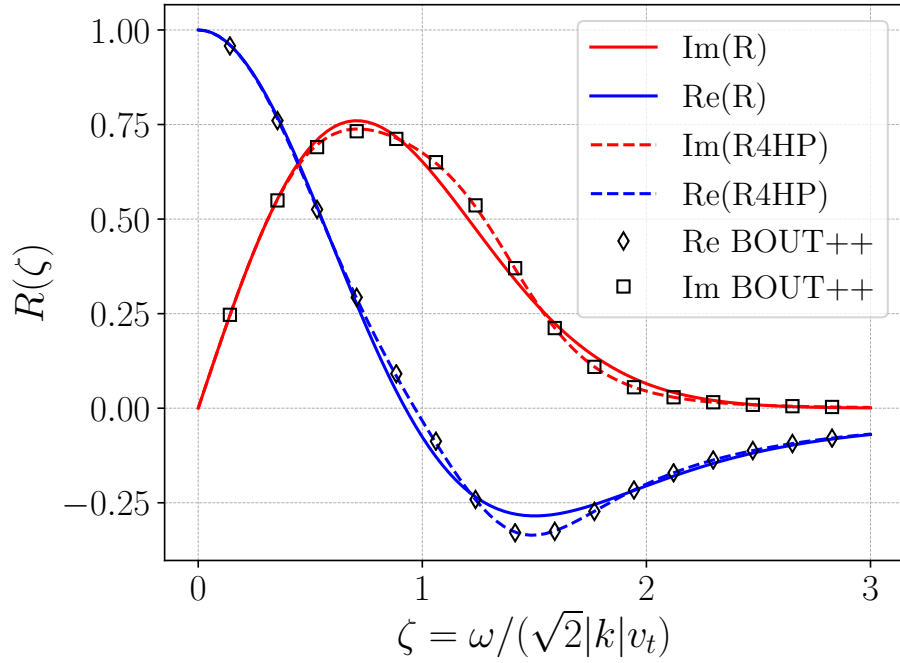


Figure 3.8: The real and imaginary parts of the normalized response function for the four-moment model (with BOUT++ non-Fourier calculations) with HP-like closure (3.19) compared to the exact response function.

scheme (3.9), our system is: (tildes and primes are omitted, system is linear and normalized)

$$\frac{\partial n}{\partial t} + \frac{\partial v}{\partial z} = 0, \quad (3.20a)$$

$$\frac{\partial v}{\partial t} + \tau \frac{\partial n}{\partial z} + \tau \frac{\partial T}{\partial z} + \frac{\partial n}{\partial z} = 0, \quad (3.20b)$$

$$\frac{\partial T}{\partial t} + 2 \frac{\partial v}{\partial z} + 2 \frac{\partial q}{\partial z} = 0, \quad (3.20c)$$

where $\tau = T_{0i}/T_{0e}$, and q is found by the non-Fourier method, Eq. (3.15). Long system length was chosen, $L = 200\lambda_D$, to satisfy condition $k\lambda_D \ll 1$. To observe damping, an initial condition of density perturbation n was imposed in the form of harmonic wave with the smallest possible wavenumber $k = 2\pi/L$.

Fig. 3.9 shows the damping rate from non-Fourier simulations (circles) for different values of τ , in comparison with the exact solution of the fluid dispersion relation (Eq. 2.49, solid line). It shows excellent agreement and therefore serves as another verification of the

implemented fast non-Fourier method. Both results are close to the exact kinetic solution from Chapter 1 (shown by dashed line).

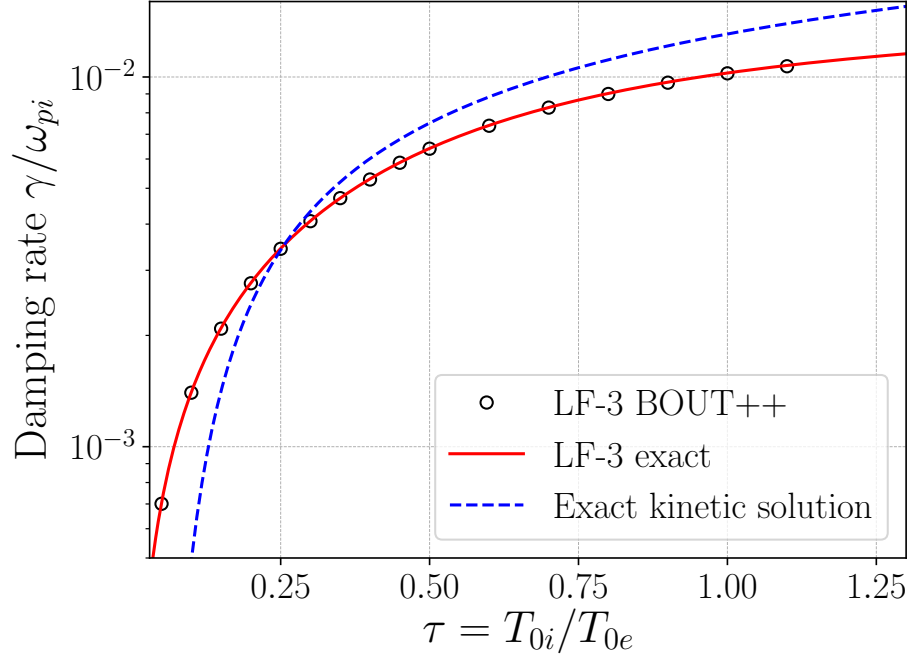


Figure 3.9: Landau damping for three-moment fluid simulation with kinetic closure. Numerical result (circles) for damping rate in comparison with exact solution of the fluid dispersion relation (2.49) (solid red). Also, the exact kinetic solution of ion Landau damping is presented (dashed blue).

CHAPTER 4

CONCLUSION

Fluid plasma equations are based on an infinite hierarchy of moments of the kinetic Vlasov equation. The full infinite system is equivalent to the kinetic equation. For practical calculations the hierarchy is truncated in one or another way, either by simply dropping higher-order terms, or providing the closures for higher moments in terms of the lower moments. In the regime of frequent collisions (short mean free path) the velocity distribution function is close to Maxwellian, and the closure can be derived using small parameters, $\lambda \ll L$ (mean free path is much shorter than the system length) and $\nu \gg \omega$ (frequent collisions), e.g. via the standard Chapman-Enskog procedure [1]. The result is classical transport theory with constant transport coefficients. Many modern plasmas of interest, e.g. in magnetic confinement devices, are almost collisionless and mean free path is large compared to the size of the device and the characteristic length of the perturbations. Yet, plasmas are confined relatively long time, therefore the lowest order distribution function is still close to Maxwellian. Then the small deviations from Maxwellian can be sought via the perturbative approach. This can be done directly in the kinetic theory or from more advanced fluid theory.

Basic plasma fluid models generally miss kinetic effects such as Landau damping. The problem of kinetic closures for fluid equations that incorporate the Landau damping is a subject of this thesis. More or less systematic approach was proposed in Hammett-Perkins [11] (HP) work. These authors came up with closures that approximate the kinetic plasma response function. A comprehensive approach leading to exact closures is described in Refs. [14, 15].

By using generalized Chapman-Enskog method [14, 15] I have derived the exact linear kinetic closure (2.37) for the three-moment plasma fluid model in the one-dimensional case. The closure variable, heat flux q (2.37) found as the complicated expression in terms of the

plasma dispersion function $Z(\zeta)$. This closure provides a linearly exact response function which is identical to the linear kinetic solution. In zeroth-order approximation it provides the same result that as was previously obtained with HP three-moment closure ansatz (2.2). By including higher-order terms, the better accuracy for the plasma response function is obtained, which is comparable to the HP four-moment fluid closure ansatz, Fig. 3.7.

Nonlocal nature of the closure operators expressed in the form of complex functions of the wave vector is impractical for nonlinear simulations, especially in complex geometries. In this thesis, I implemented collisionless closure operators in a numerical model by using a recently proposed [12] non-Fourier method. It approximates the closure term by a sum of Lorentzians in Fourier space. The latter corresponds to the solution of the modified Helmholtz equation in real space. The whole procedure was numerically implemented in the BOUT++ framework [48]. The one-dimensional plasma density response function both in our BOUT++ implementation and the Fourier analysis has shown excellent agreement (Fig. 3.6) with exact response function for real frequencies (neglecting the mode growth and damping). The same calculations were performed for a four-moment model with a closure for r variable, proposed by HP, also showing excellent agreement (Fig. 3.8) with the analytical plasma response function.

The obtained collisionless kinetic closure was also verified in a self-consistent model of the ion Landau damping in BOUT++. It was done with the three-moment fluid system and HP-like closure for the heat flux. The same fast non-Fourier method has been used for the closure operator calculation. The resulting damping rate (shown in Fig. 3.9) agrees well with the theoretical results.

The future work can be focused on a generalizing of the fast non-Fourier method. As I shown in this thesis, the higher-order terms in the heat flux closure improve the agreement with kinetic theory. The higher-order terms include the frequency dependence which can be converted into the real space and time domain with additional time derivatives. Such a system of fluid equations with closures that involve time derivatives can also be modeled within the BOUT++ framework.

Despite the limitations, linear closures are being used in nonlinear plasma fluid simulations. Our results and practical implementations in BOUT++ can be used in such problems,

e.g., for the problem of the instability and transport due to lower-hybrid modes [49] relevant to $\mathbf{E} \times \mathbf{B}$ plasmas and electric propulsion and plasma processing devices [50].

REFERENCES

- [1] S. Chapman and T.G. Cowling. *The mathematical theory of non-uniform gases: an account of the kinetic theory of viscosity, thermal conduction and diffusion in gases.* Cambridge University Press, 1970.
- [2] S.I. Braginskii. Transport processes in a plasma. *Reviews of Plasma Physics*, 1:205, 1965.
- [3] T.H. Stix. *Waves in plasmas.* Springer, 1992.
- [4] G.F. Chew, M.L. Goldberger, and F.E. Low. The Boltzmann equation and the one-fluid hydromagnetic equations in the absence of particle collisions. *Proceedings of the Royal Society of London A: Mathematical, Physical and Engineering Sciences*, 236(1204):112–118, 1956.
- [5] F.L. Hinton and R.D. Hazeltine. Theory of plasma transport in toroidal confinement systems. *Reviews of Modern Physics*, 48(2):239, 1976.
- [6] C.K. Birdsall. Particle-in-cell charged-particle simulations, plus Monte Carlo collisions with neutral atoms, PIC-MCC. *IEEE Transactions on Plasma Science*, 19(2):65–85, 1991.
- [7] J.P. Verboncoeur. Particle simulation of plasmas: review and advances. *Plasma Physics and Controlled Fusion*, 47(5A):A231, 2005.
- [8] H.C. Kim, F. Iza, S.S. Yang, M. Radmilović-Radjenović, and J.K. Lee. Particle and fluid simulations of low-temperature plasma discharges: benchmarks and kinetic effects. *Journal of Physics D: Applied Physics*, 38(19):R283, 2005.
- [9] G.S. Lee and P.H. Diamond. Theory of ion-temperature-gradient-driven turbulence in tokamaks. *Physics of Fluids*, 29(10):3291–3313, 1986.
- [10] S. Hamaguchi and W. Horton. Effects of sheared flows on ion-temperature-gradient-driven turbulent transport. *Physics of Fluids B: Plasma Physics*, 4(2):319–328, 1992.
- [11] G.W. Hammett and F.W. Perkins. Fluid moment models for Landau damping with application to the ion-temperature-gradient instability. *Physical Review Letters*, 64:3019–3022, Jun 1990.
- [12] A.M. Dimits, I. Joseph, and M.V. Umansky. A fast non-Fourier method for Landau-fluid operators. *Physics of Plasmas*, 21(5):055907, 2014.

- [13] B.D. Dudson, M.V. Umansky, X.Q. Xu, P.B. Snyder, and H.R. Wilson. BOUT++: A framework for parallel plasma fluid simulations. *Computer Physics Communications*, 180(9):1467–1480, 2009.
- [14] Z. Chang and J.D. Callen. Unified fluid/kinetic description of plasma microinstabilities. part I: Basic equations in a sheared slab geometry. *Physics of Fluids B: Plasma Physics*, 4(5):1167–1181, 1992.
- [15] S.K. Litt, A.I. Smolyakov, E. Hassan, and W. Horton. Ion thermal and dispersion effects in Farley-Buneman instabilities. *Physics of Plasmas*, 22(8):082112, 2015.
- [16] A.A. Vlasov. On vibration properties of electron gas. *Journal of Experimental and Theoretical Physics*, 8(3):291, 1938.
- [17] Y.L. Klimontovich. *The Statistical Theory of Non-Equilibrium Processes in a Plasma: International Series of Monographs in Natural Philosophy*, volume 9. Elsevier, 2013.
- [18] N.N. Bogolyubov. Dynamic theory problems in statistical physics. *Gostekhizdat, Moscow, Leningrad*, 1946.
- [19] M. Born. *A General kinetic theory of liquids*. Cambridge University Press, 1949.
- [20] J.G. Kirkwood. The statistical mechanical theory of transport processes I. General theory. *The Journal of Chemical Physics*, 14(3):180–201, 1946.
- [21] J.G. Kirkwood. The statistical mechanical theory of transport processes II. Transport in gases. *The Journal of Chemical Physics*, 15(1):72–76, 1947.
- [22] J. Yvon. *La théorie statistique des fluides et l'équation d'état*, volume 203. Hermann et Cie, 1935.
- [23] F.H. Harlow and M.W. Evans. A machine calculation method for hydrodynamic problems. *LAMS-1956*, 1955.
- [24] L.D. Landau. On the vibrations of the electronic plasma. *Zh. Eksp. Teor. Fiz.*, 10:25, 1946.
- [25] J.R. Pierce. Possible fluctuations in electron streams due to ions. *Journal of Applied Physics*, 19(3):231–236, 1948.
- [26] C.K. Birdsall and A.B. Langdon. *Plasma physics via computer simulation*. CRC Press, 2004.
- [27] C.K. Birdsall et al. XES1: 1D particle-in-cell code for periodic domain. <http://ptsg.eecs.berkeley.edu/>, 1993–.
- [28] J.P. Boris. Acceleration calculation from a scalar potential. Technical report, Princeton Univ., NJ Plasma Physics Lab., 1970.
- [29] F.F. Chen. *Introduction to plasma physics*. Springer, 2012.

- [30] J.A. Bittencourt. *Fundamentals of plasma physics*. Springer, 2013.
- [31] H. Grad. On the kinetic theory of rarefied gases. *Communications on pure and applied mathematics*, 2(4):331–407, 1949.
- [32] A.V. Bobylev. The Chapman-Enskog and Grad methods for solving the Boltzmann equation. *Akademiia Nauk SSSR Doklady*, 262:71–75, 1982.
- [33] A.B. Mikhailovskii and V.S. Tsypin. Transport equations of plasma in a curvilinear magnetic field. *Contributions to Plasma Physics*, 24(4):335–354, 1984.
- [34] A.I. Smolyakov, M. Yagi, and J.D. Callen. Nonlocal closures in long mean free path regimes. *Topics in Kinetic Theory*, 46:243, 2005.
- [35] A. Fick. On liquid diffusion. *Philosophical Magazine*, 10(63):30–39, 1855.
- [36] A.A. Vlasov. On the kinetic theory of an assembly of particles with collective interaction. *Russian Physics Journal*, 9:25–40, 1945.
- [37] B.D. Fried and S.D. Conte. *The plasma dispersion function: the Hilbert transform of the Gaussian*. Academic Press, 2015.
- [38] B.B. Kadomtsev and O.P. Pogutse. Proceedings of the International Conference on Plasma Physics and Controlled Nuclear Fusion Research. 2:69, 1985.
- [39] R.E. Waltz. Three-dimensional global numerical simulation of ion temperature gradient mode turbulence. *The Physics of Fluids*, 31(7):1962–1967, 1988.
- [40] A.M. Dimits, I. Joseph, M.V. Umansky, P.W. Xi, and X.Q. Xu. Efficient non-Fourier implementation of Landau-fluid operators in the BOUT++ code. *APS Meeting Abstracts*, 2012.
- [41] X.Q. Xu, P.W. Xi, A. Dimits, I. Joseph, M.V. Umansky, T.Y. Xia, B. Gui, S.S. Kim, G.Y. Park, T. Rhee, et al. Gyro-fluid and two-fluid theory and simulations of edge-localized-modes. *Physics of Plasmas*, 20(5):056113, 2013.
- [42] B.D. Dudson, A. Allen, G. Breyiannis, E. Brugger, J. Buchanan, L. Easy, S. Farley, I. Joseph, M. Kim, A.D. McGann, et al. BOUT++: Recent and current developments. *Journal of Plasma Physics*, 81(01):365810104, 2015.
- [43] X.Q. Xu and R.H. Cohen. Scrape-Off Layer Turbulence Theory and Simulations. *Contributions to Plasma Physics*, 38(1-2):158–170, 1998.
- [44] M.V. Umansky, X.Q. Xu, B.D. Dudson, L.L. LoDestro, and J.R. Myra. Status and verification of edge plasma turbulence code BOUT. *Computer Physics Communications*, 180(6):887–903, 2009.
- [45] B.D. Dudson and M.V. Umansky. BOUT++: Framework for fluid and plasma simulations in curvilinear geometry. <http://boutproject.github.io/>, 2008–.

- [46] J.D. Anderson and J. Wendt. *Computational fluid dynamics*, volume 206. Springer, 1995.
- [47] Suite of Nonlinear and Differential/Algebraic Equation Solvers. <https://computation.llnl.gov/projects/sundials>.
- [48] O. Chapurin, A.I. Smolyakov, and M.V. Umansky. Landau-fluid closures and their implementation in BOUT++ with non-Fourier methods. *International Conference on Plasma Science*, Jun. 19-23 2016.
- [49] A.I. Smolyakov, O. Chapurin, W. Frias, O. Koshkarov, I. Romadanov, T. Tang, M.V. Umansky, Y. Raitses, I.D. Kaganovich, and V.P. Lakhin. Fluid theory and simulations of instabilities, turbulent transport and coherent structures in partially-magnetized plasmas of discharges. *Plasma Physics and Controlled Fusion*, 59(1):014041, 2016.
- [50] O. Chapurin and A.I. Smolyakov. On the electron drift velocity in plasma devices with $E \times B$ drift. *Journal of Applied Physics*, 119(24):243306, 2016.
- [51] L.C. Andrews. *Special functions of mathematics for engineers*. 1992.
- [52] J. Eric, O. Travis, P. Pearu, et al. SciPy: Open source scientific tools for Python. <http://www.scipy.org/>, 2001–.
- [53] G.J. Steven. Faddeeva W function implementation. <http://ab-initio.mit.edu/Faddeeva>.

APPENDIX A

GENERALIZED CLOSURE FOR THE VISCOSITY AND HEAT FLUX IN 3D CASE

In this Appendix, the review of the exact closure models following to Chang-Callen [14] (CC) and Litt-Smolyakov [15] (LS) studies is given. The purpose of this Appendix is to compare the CC and LS results. It will be shown that CC closure has some inconsistency in provided results, more specifically with obtaining the exact plasma response function. Both CC and LS approaches are based on the Chapman-Enskog method [1]. Following the Chapman-Enskog ansatz, the distribution function f is represented in the form:

$$f = F_M + \tilde{F}, \quad (\text{A.1})$$

where F_M is the dynamical Maxwellian distribution, and \tilde{F} is the deviation from the distribution. The dynamical Maxwellian is given by

$$F_M(\mathbf{x}, \mathbf{v}, t) = \frac{n(\mathbf{x}, t)}{\pi^{3/2} [2T(\mathbf{x}, t)/m]^{3/2}} \exp\left(-\frac{m [(\mathbf{v} - \mathbf{V}(\mathbf{x}, t))]^2}{2T(\mathbf{x}, t)}\right), \quad (\text{A.2})$$

and its evolution depends on the evolution of the macroscopic variables $n(x, t)$, $\mathbf{V}(x, t)$ and $T(x, t)$, where \mathbf{v} is the particle velocity and \mathbf{V} is the fluid velocity. The ansatz (A.1) also imposes the following constraints on the deviation of the distribution \tilde{F} :

$$\int \tilde{F} \left\{ 1, \mathbf{v}', mv'^2/2 \right\} d^3\mathbf{v}' = 0, \quad (\text{A.3})$$

where $\mathbf{v}' = \mathbf{v} - \mathbf{V}$ is the random velocity, and weighting functions (in the curly brackets) corresponds to the particle, momentum and energy moments. It means that \tilde{F} will not contribute to the perturbation of these lowest moments. Substituting the ansatz (A.1) in the Boltzmann equation (1.10), it can be rewritten in the form:

$$\begin{aligned} & \left(\frac{\partial n}{\partial t} + \mathbf{v} \cdot \nabla n \right) \frac{F_M}{n} + \left(\frac{\partial T}{\partial t} + \mathbf{v} \cdot \nabla T \right) \left(-\frac{3}{2} + \frac{v'^2}{v_T^2} \right) \frac{F_M}{T} \\ & + \left(\frac{\partial \mathbf{V}}{\partial t} + \mathbf{v} \cdot \nabla \mathbf{V} \right) \cdot \frac{2\mathbf{v}'}{v_T^2} F_M + \frac{e}{m} \mathbf{E} \cdot \frac{\partial F_M}{\partial \mathbf{v}} + D\tilde{F} = C(f), \end{aligned} \quad (\text{A.4})$$

where $v_T^2 = 2T/m$ is the thermal velocity and

$$D \equiv \frac{\partial}{\partial t} + \mathbf{v} \cdot \nabla + \frac{e}{m} \mathbf{E} \cdot \frac{\partial}{\partial \mathbf{v}}. \quad (\text{A.5})$$

It can be noted, that kinetic equation (A.4) contains a time evolution of the plasma fluid equations. The standard plasma fluid equations (obtained as first three moments of the kinetic equation in Chapter 1) are

$$\frac{\partial n}{\partial t} + \nabla \cdot n\mathbf{V} = 0, \quad (\text{A.6a})$$

$$mn \left(\frac{\partial \mathbf{V}}{\partial t} + \mathbf{V} \cdot \nabla \mathbf{V} \right) = -\nabla p + en\mathbf{E} - \nabla \cdot \mathbf{\Pi} + \mathbf{R}, \quad (\text{A.6b})$$

$$\frac{3}{2}n \left(\frac{\partial T}{\partial t} + \mathbf{V} \cdot \nabla T \right) = -p\nabla \cdot \mathbf{V} - \mathbf{\Pi} : \nabla \mathbf{V} - \nabla \cdot \mathbf{q} + Q, \quad (\text{A.6c})$$

with \mathbf{R} and Q :

$$\mathbf{R} = -\nu mn\mathbf{V}, \quad (\text{A.7})$$

$$Q = -\nu n \left(\frac{3}{2}(T - T_n) - \frac{m}{2}u^2 \right), \quad (\text{A.8})$$

where \mathbf{R} is the collisional term (ion-neutral collisions) and Q represents a balance between the ion frictional heating and cooling, caused by collisions. Including macroscopic evolution equations (A.6) into Eq. (A.4) one obtains the recast of kinetic equation in the Chapman-Enskog form:

$$\begin{aligned} D\tilde{F} &= C(f) + \mathbf{v}' \cdot \nabla T \left(\frac{5}{2} - \frac{v'^2}{v_T^2} \right) \frac{F_M}{T} - \left(\mathbf{v}' \mathbf{v}' - \frac{v'^2}{3} \mathbf{I} \right) : \nabla \mathbf{V} m \frac{F_M}{T} \\ &- (\mathbf{\Pi} : \nabla \mathbf{V} + \nabla \cdot \mathbf{q} - Q) \left(1 - \frac{2}{3} \frac{v'^2}{v_T^2} \right) \frac{F_M}{p} + (\nabla \cdot \mathbf{\Pi} - \mathbf{R}) \cdot \mathbf{v}' \frac{F_M}{p}, \end{aligned} \quad (\text{A.9})$$

where the deviation \tilde{F} depends on the lower order moments. This equation is still fully equivalent to linearized Boltzmann equation (1.10).

At this point one-dimensional problem is considered, in the direction of the perturbed electric field (and the wavevector). After linearizing the Chapman-Enskog-like equation A.9 for \tilde{F} and taking the Fourier transform of Eq. (A.9) (using $\partial/\partial t \rightarrow -i\omega$ and $\nabla \rightarrow ik_{\parallel}$), one obtains

$$\begin{aligned} \tilde{F} &= \frac{\tilde{V}_{\parallel}}{v_T} \frac{4}{3} \frac{k_{\parallel} v_T F_M}{\omega + i\nu - k_{\parallel} v'_{\parallel}} \left(\frac{v_{\parallel}^2}{v_T^2} - \frac{v_{\perp}^2}{2v_T^2} \right) - \frac{\tilde{\Pi}_{\parallel}}{p} \frac{k_{\parallel} v'_{\parallel} F_M}{\omega + i\nu - k_{\parallel} v'_{\parallel}} \\ &+ \frac{\tilde{q}_{\parallel}}{p v_T} \frac{2}{3} \frac{k_{\parallel} v_T F_M}{\omega + i\nu - k_{\parallel} v'_{\parallel}} L_1^{(1/2)}(x) - \frac{\tilde{T}}{T} \frac{k_{\parallel} v'_{\parallel} F_M}{\omega + i\nu - k_{\parallel} v'_{\parallel}} L_1^{(3/2)}(x), \end{aligned} \quad (\text{A.10})$$

with $L_1^{(1/2)}(x) = 3/2 - v'^2/v_T^2$ and $L_1^{(3/2)}(x) = 5/2 - v'^2/v_T^2$, and the moments \tilde{V}_\parallel , $\tilde{\Pi}_\parallel$ and \tilde{q}_\parallel are defined with respect to the direction of wavevector. The following identities have been used:

$$\left(\mathbf{v}'\mathbf{v}' - \frac{v'^2}{3}\mathbf{I}\right) : \nabla\mathbf{V} = \frac{2}{3}ik_\parallel V_\parallel \left(v_\parallel'^2 - v_\perp'^2/2\right), \quad (\text{A.11})$$

and

$$\nabla \cdot \mathbf{\Pi} \cdot \mathbf{v}' = ik_\parallel \Pi_\parallel v_\parallel', \quad (\text{A.12})$$

where V_\parallel and Π_\parallel are the components along the perturbed ion velocity; in case of $\mathbf{k} = k_x \hat{\mathbf{x}}$, these would be V_x and Π_{xx} , respectively. The Eq. (A.10) for \tilde{F} can be written in the short form as

$$\tilde{F} = \frac{\tilde{V}_\parallel}{v_T} a_V - \frac{\tilde{\Pi}_\parallel}{p} a_\pi + \frac{\tilde{q}_\parallel}{pv_T} a_q - \frac{\tilde{T}}{T} a_T, \quad (\text{A.13})$$

with the following coefficients:

$$a_V = \frac{4}{3} \frac{k_\parallel v_T F_M}{\omega + i\nu - k_\parallel v_\parallel'} \left(\frac{v_\parallel'^2}{v_T^2} - \frac{v_\perp'^2}{2v_T^2} \right), \quad (\text{A.14})$$

$$a_\pi = \frac{k_\parallel v_\parallel' F_M}{\omega + i\nu - k_\parallel v_\parallel'}, \quad (\text{A.15})$$

$$a_q = \frac{2}{3} \frac{k_\parallel v_T F_M}{\omega + i\nu - k_\parallel v_\parallel'} L_1^{(1/2)}(x), \quad (\text{A.16})$$

$$a_T = \frac{k_\parallel v_\parallel' F_M}{\omega + i\nu - k_\parallel v_\parallel'} L_1^{(3/2)}(x). \quad (\text{A.17})$$

Previously imposed constraint (A.3) on the deviation \tilde{F} state that it is not affected by the lowest moments. Therefore, by integrating Eq. (A.13) with $\{1, \mathbf{v}', mv'^2/2\}$ moments, one can obtain

$$\frac{\tilde{\Pi}_\parallel}{p_0} = P_V \frac{\tilde{V}_\parallel}{v_T} + P_T \frac{\tilde{T}}{T_0}, \quad (\text{A.18})$$

$$\frac{\tilde{q}_\parallel}{p_0 v_T} = Q_V \frac{\tilde{V}_\parallel}{v_T} + Q_T \frac{\tilde{T}}{T_0}, \quad (\text{A.19})$$

where closure coefficients P_V, P_T, Q_V, Q_T are complex functions of the plasma dispersion function $Z(\zeta)$ with a complex argument $\zeta = (\omega + i\nu)/(k_\parallel v_T)$. It can be noted, that obtained closures have the Onsager symmetry properties, i.e. they are both expressed as the functions of \tilde{V} and \tilde{T} .

Obtained above form of closure expressions is similar in both Chang-Callen and Litt-Smolyakov works. One can check that these closures, used with the plasma fluid equations, provide the same linear kinetic response function $R(\zeta) = 1 + \zeta Z(\zeta)$. First, the plasma response function can be represented in general depending on coefficients P_V, P_T, Q_V, Q_T . Then the corresponding coefficients from CC and LS results can be substituted for comparison between each other. The plasma response function appeared in $\tilde{n} = qn_0/T_0 R\tilde{\phi}$, and, therefore, can be expressed from the linearized fluid equations (A.6):

$$-i w \tilde{n} + i k n_0 \tilde{u} = 0, \quad (\text{A.20a})$$

$$-i w m n_0 \tilde{u} = -i k n_0 \tilde{T} - i k T_0 \tilde{n} - i k e n_0 \tilde{\phi} - i k \tilde{\pi}, \quad (\text{A.20b})$$

$$-\frac{3}{2} i w n_0 \tilde{T} = -i k n_0 T_0 \tilde{u} - i k \tilde{q}. \quad (\text{A.20c})$$

After substitution of obtained closures for π (A.18) and q (A.19) and solving the system (A.20), one can find the response function, expressed via P_V, P_T, Q_V, Q_T coefficients:

$$R = \frac{2Q_t - 3\zeta}{2Q_t - 2\zeta (P_t Q_v - P_v Q_t + Q_v + P_t + 4) - \zeta^2 (4Q_t + 3P_v) + 6\zeta^3}. \quad (\text{A.21})$$

Let us start with the Chang-Callen results. Denoting with the upper *cc* index, closure coefficients for the linear closure terms (A.18,A.19) are presented as functions of Z and ζ :

$$P_V^{cc} = \frac{6Z(2Z\zeta^2 - Z + 2\zeta)}{4Z^2\zeta - 2Z\zeta^2 + 5Z - 2\zeta}, \quad (\text{A.22a})$$

$$P_T^{cc} = -\frac{4Z^2\zeta + 4Z\zeta^2 + 2Z + 4\zeta}{\frac{8}{3}Z^2\zeta - \frac{4}{3}Z\zeta^2 + \frac{10}{3}Z - \frac{4}{3}\zeta}, \quad (\text{A.22b})$$

$$Q_V^{cc} = -\frac{4Z^2\zeta + 4Z\zeta^2 + 2Z + 4\zeta}{4Z^2\zeta - 2Z\zeta^2 + 5Z - 2\zeta}, \quad (\text{A.22c})$$

$$Q_T^{cc} = \frac{12Z^2\zeta^2 - 6Z\zeta^3 + 33Z\zeta - 6\zeta^2 + 18}{8Z^2\zeta - 4Z\zeta^2 + 10Z - 4\zeta}. \quad (\text{A.22d})$$

By substituting them into Eq. (A.21) one obtains the following expression for the response function:

$$R_3^{cc} = \frac{Z\zeta + 1}{1 - \frac{1}{3}Z\zeta + \frac{2}{3}\zeta^2 + \frac{2}{3}Z\zeta^3}, \quad (\text{A.23})$$

which is not the expected exact response function (1.81). For a small argument approximation the obtained result gives $R_3^{cc} \approx 1 + \frac{4}{3}i\zeta\sqrt{\pi}$, where the distinction with the exact small argument limit (1.82) is present already in the first order term. This can be explained with

the typo in CC work. For further comparison, let us present here expansions for closure coefficients in CC work. The cold plasma limit $\zeta \ll 1$ approximation results into:

$$P_V^{cc} = -\frac{6}{5}i\sqrt{\pi} + \zeta \left(-\frac{24}{25}\sqrt{\pi}^2 + \frac{108}{25} \right), \quad (\text{A.24a})$$

$$P_T^{cc} = -\frac{3}{5} + \zeta \left(-\frac{18}{25}i\sqrt{\pi} + \frac{36i}{25\sqrt{\pi}} \right), \quad (\text{A.24b})$$

$$Q_V^{cc} = -\frac{2}{5} + \zeta \left(-\frac{12}{25}i\sqrt{\pi} + \frac{24i}{25\sqrt{\pi}} \right), \quad (\text{A.24c})$$

$$Q_T^{cc} = -\frac{9i}{5\sqrt{\pi}} + \zeta \left(\frac{93}{50} - \frac{108}{25\pi} \right). \quad (\text{A.24d})$$

In the hot plasma approximation $\zeta \gg 1$:

$$P_V^{cc} = 2\zeta^{-1} + \frac{7}{3}\zeta^{-3}, \quad (\text{A.25a})$$

$$P_T^{cc} = \zeta^{-2} + \frac{11}{3}\zeta^{-4}, \quad (\text{A.25b})$$

$$Q_V^{cc} = \frac{2}{3}\zeta^{-2} + \frac{22}{9}\zeta^{-4}, \quad (\text{A.25c})$$

$$Q_T^{cc} = \frac{5}{4}\zeta^{-1} + \frac{7}{3}\zeta^{-3}. \quad (\text{A.25d})$$

For Litt-Smolyakov results any indices are omitted in the following notation. The coefficients for closure terms (A.18, A.19), expressed in terms of the plasma dispersion function Z and ζ are

$$P_V = \frac{Z(12Z\zeta^2 - 6Z + 12\zeta)}{6Z^2\zeta - 3Z\zeta^2 + 7.5Z - 3\zeta}, \quad (\text{A.26a})$$

$$P_T = \frac{4Z^2\zeta + 4Z\zeta^2 + 2Z + 4\zeta}{-4Z^2\zeta + 2Z\zeta^2 - 5Z + 2\zeta}, \quad (\text{A.26b})$$

$$Q_V = \frac{2Z^2\zeta + 2Z\zeta^2 + 1Z + 2\zeta}{-2Z^2\zeta + Z\zeta^2 - 2.5Z + 1\zeta}, \quad (\text{A.26c})$$

$$Q_T = \frac{-6Z^2\zeta^2 + 3Z\zeta^3 - 16.5Z\zeta + 3\zeta^2 - 9}{-4Z^2\zeta + 2Z\zeta^2 - 5Z + 2\zeta}. \quad (\text{A.26d})$$

By substituting LS coefficients (A.26) into the general expression for response function (A.21), one obtains

$$R_3 = 1 + \zeta Z, \quad (\text{A.27})$$

which is fully equivalent to the exact kinetic linear response function (1.81), as expected. Let

us approximate the coefficients (A.26) in $\zeta \ll 1$ limit:

$$P_V = -\frac{4}{5}i\sqrt{\pi} + \zeta \left(-\frac{16}{25}\pi + \frac{72}{25} \right), \quad (\text{A.28a})$$

$$P_T = -\frac{2}{5} + \zeta \left(-\frac{12}{25}i\sqrt{\pi} + \frac{24}{25}\frac{i}{\sqrt{\pi}} \right), \quad (\text{A.28b})$$

$$Q_V = -\frac{2}{5} + \zeta \left(-\frac{12}{25}i\sqrt{\pi} + \frac{24}{25}\frac{i}{\sqrt{\pi}} \right), \quad (\text{A.28c})$$

$$Q_T = -\frac{9i}{5\sqrt{\pi}} + \zeta \left(\frac{93}{50} - \frac{108}{25\pi} \right). \quad (\text{A.28d})$$

By substituting only zeroth-order terms (terms without ζ) of coefficients (A.28) into Eq. (A.21) and solving for response function, one obtains the following result:

$$R_3 \approx \frac{25\sqrt{\pi}\zeta + 30i}{31\sqrt{\pi}\zeta - 2\zeta(2i\sqrt{\pi} + 5\zeta)(5\sqrt{\pi}\zeta + 6i) + 30i}, \quad (\text{A.29})$$

where the small term approximation (1.78) for dispersion function $Z(\zeta)$ is used. Expanding (A.29) with small argument ζ will give

$$R_3 \approx 1 + i\sqrt{\pi}\zeta + \left(2 - \frac{7}{6}\pi \right) \zeta^2, \quad (\text{A.30})$$

which is consistent with the exact response function expansion (1.82) for the first order. Expanding the obtained response function (A.29) with a large argument ζ leads to

$$R_3 \approx -\frac{1}{2}\zeta^{-2} + \frac{1}{5}i\sqrt{\pi}\zeta^{-3}, \quad (\text{A.31})$$

which is also consistent with the exact formula expansion in Eq. (1.83) for the second order; ζ^{-3} term is absent in exact expansion of response function. The illustration can be seen in Fig. A.1, where the R_3 (A.29) and the Hammett-Perkins result for three-moment closure ansatz (2.5) are compared with the exact result. In the limit of high collisionality ($\zeta \gg 1$), LS coefficients (A.26) appeared as

$$P_V = \frac{4}{3}\zeta^{-1} + \frac{14}{9}\zeta^{-3}, \quad (\text{A.32a})$$

$$P_T = \frac{2}{3}\zeta^{-2} + \frac{22}{9}\zeta^{-4}, \quad (\text{A.32b})$$

$$Q_V = \frac{2}{3}\zeta^{-2} + \frac{22}{9}\zeta^{-4}, \quad (\text{A.32c})$$

$$Q_T = \frac{5}{4}\zeta^{-1} + \frac{7}{3}\zeta^{-3}. \quad (\text{A.32d})$$

By substituting only first terms (terms with ζ^{-1} and ζ^{-2}) of coefficients (A.32) into Eq. (A.21) and solving for response function, one obtains the following result:

$$R_3 = -\frac{9\zeta^2(6\zeta^2 - 5)}{108\zeta^6 - 252\zeta^4 + 57\zeta^2 - 16}, \quad (\text{A.33})$$

where $Z(\zeta)$ was replaced the expression for the large argument approximation of $Z(\zeta)$ (1.79). Expanding the obtained response with a large ζ results in

$$R \approx -\frac{1}{2}\zeta^{-2} + \frac{5}{12}\zeta^{-4}, \quad (\text{A.34})$$

which is consistent with the exact response function expansion in Eq. (1.83).

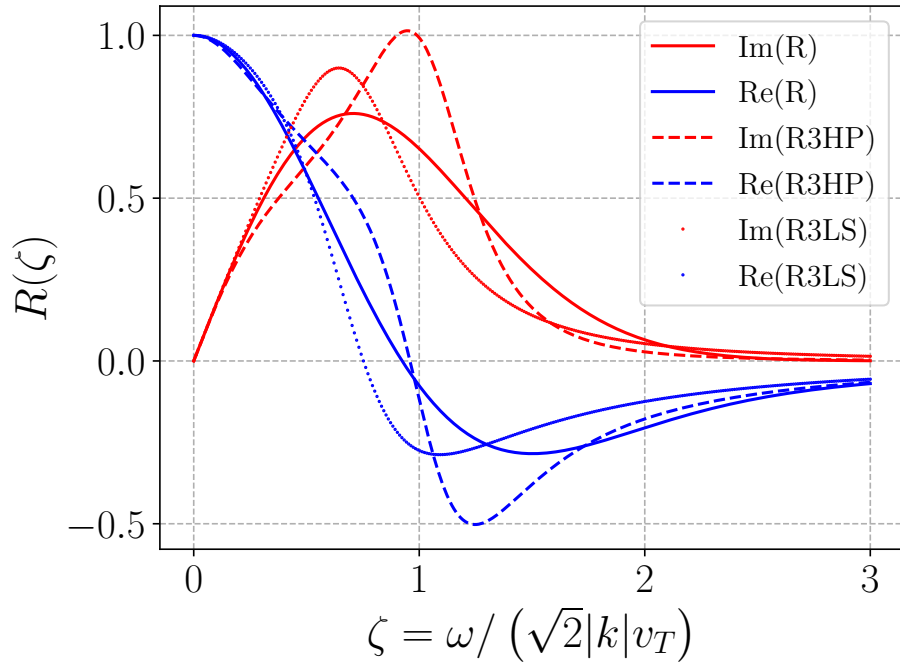


Figure A.1: The real and imaginary parts of the normalized plasma response function. Three-moment model with Litt-Smolyakov closure (A.29) response function R3LS (dotted) is compared to the Hammett-Perkins three-moment response function result R3HP (dashed). The exact plasma response function R is also present (solid).

APPENDIX B

PLASMA DISPERSION FUNCTION

Plasma dispersion function is a special function of a complex argument. It appears in many areas of plasma physics, particularly, in application to the collisionless kinetic equation. In this thesis I have used mostly the plasma response function $R = 1 + \zeta Z$, expressed through the plasma dispersion function Z . Thus, the central point is the evaluation of the plasma dispersion function Z . The plasma dispersion function was already defined (1.75), but another definition [37] can be used:

$$Z(\zeta) = 2ie^{-\zeta^2} \int_{-\infty}^{i\zeta} e^{-t^2} dt, \quad (\text{B.1})$$

which is valid for any sign of $\text{Im } \zeta$. It also can be related to the error function, and, in fact,

$$Z(\zeta) = i\sqrt{\pi}e^{-\zeta^2} \text{erfc}(-i\zeta), \quad (\text{B.2})$$

where erfc is the complementary error function [51].

The SciPy [52] (library for Python) has been used in my numerical calculations, where the special function w represents the Fadeev function:

$$w(z) = e^{-\zeta^2} \text{erfc}(-i\zeta). \quad (\text{B.3})$$

It can be seen that $Z(\zeta) = i\sqrt{\pi}w(\zeta)$. The details on the algorithms and the code behind the implementation of the Fadeev function can be found in Ref. [53]. The code is also available for C, Matlab, GNU Octave, R, Scilab, and Julia.

To illustrate a general behavior of the plasma dispersion function, the plots can be found in Figs. B.1-B.3. They are all consistent with the well-known work of Fried-Conte [37].

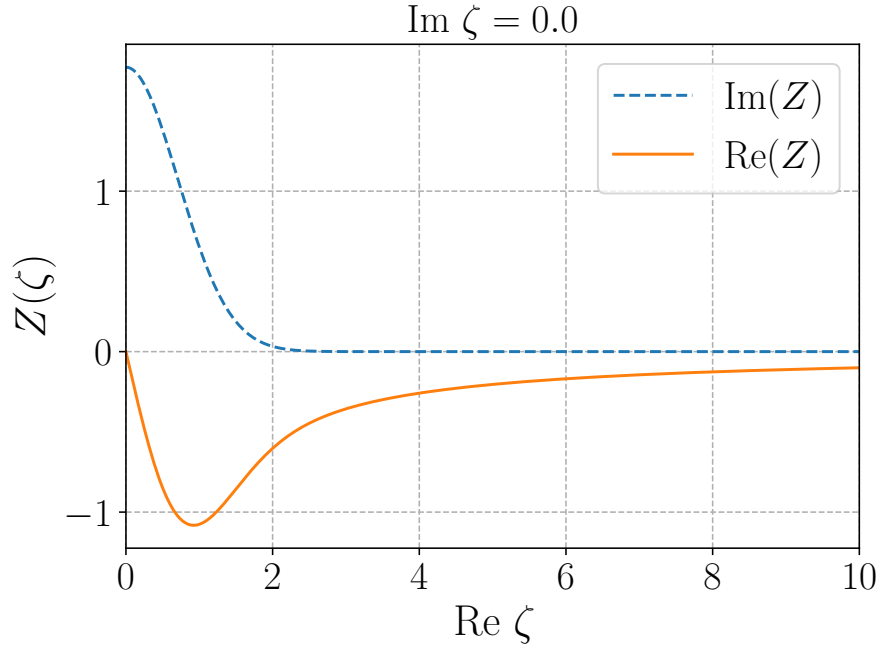


Figure B.1: Plasma dispersion function for the real argument.

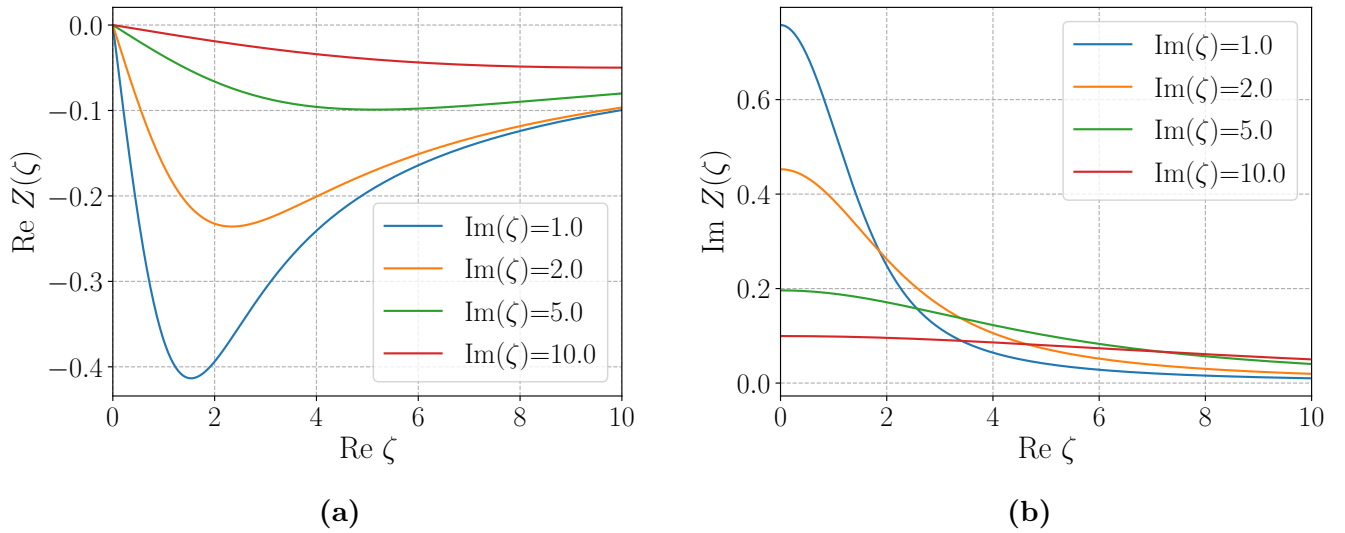


Figure B.2: Plasma dispersion function for the complex argument with positive imaginary values; (a) shows the real output and (b) shows the imaginary output.

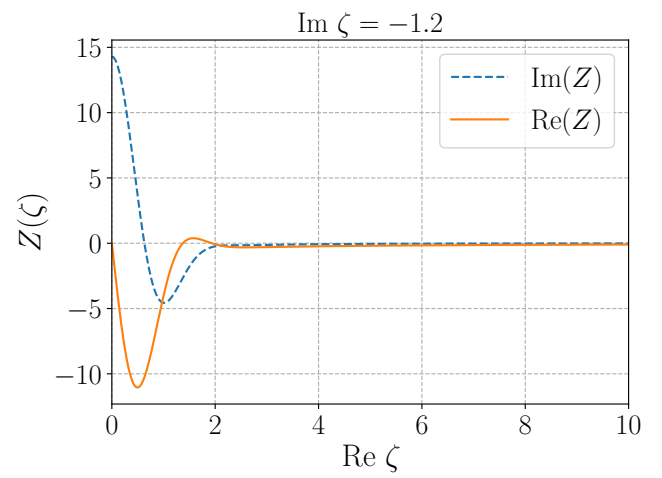
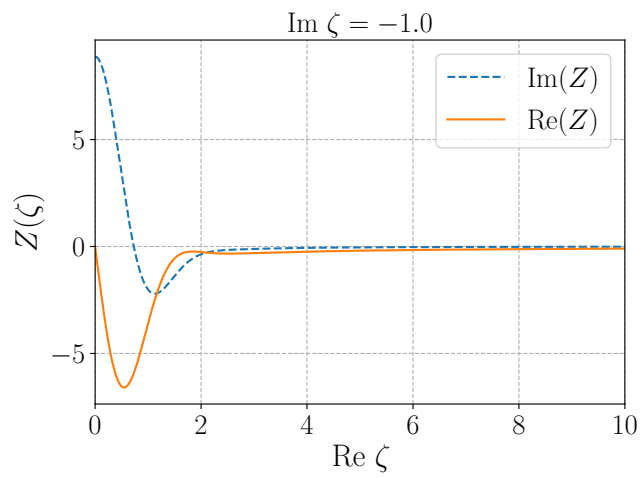


Figure B.3: Plasma dispersion function for the complex argument with negative imaginary values.

APPENDIX C

VELOCITY WEIGHTED INTEGRALS OF THE MAXWELLIAN IN TERMS OF PLASMA DISPERSION FUNCTION

The integrals used to evaluate the coefficients in Chapter 2 defined as

$$F_0 = \frac{1}{\sqrt{\pi}v_T} \exp\left(-\frac{v'^2}{v_T^2}\right), \quad (\text{C.1})$$

$$\int_{-\infty}^{\infty} F_0 \, dv' = 1, \quad (\text{C.2})$$

$$\int_{-\infty}^{\infty} v'^2 F_0 \, dv' = \frac{v_T^2}{2}, \quad (\text{C.3})$$

$$\int_{-\infty}^{\infty} \frac{dv'}{\omega - kv'} F_0 = -\frac{1}{kv_T} Z(\zeta), \quad (\text{C.4})$$

$$\int_{-\infty}^{\infty} \frac{v' dv'}{\omega - kv'} F_0 = -\frac{1}{k} (1 + \zeta Z(\zeta)), \quad (\text{C.5})$$

$$\int_{-\infty}^{\infty} \frac{v'^2 dv'}{\omega - kv'} F_0 = -\frac{v_T}{k} \zeta (1 + \zeta Z(\zeta)), \quad (\text{C.6})$$

$$\int_{-\infty}^{\infty} \frac{v'^3 dv'}{\omega - kv'} F_0 = -\frac{v_T^2}{k} \left(\frac{1}{2} + \zeta^2 (1 + \zeta Z(\zeta)) \right). \quad (\text{C.7})$$